PEOPLE'S DEMOCRATIC REPUBLIC OF ALGERIA

Ministry of Higher Education and Scientific Research

**University of Amar Telidji - Laghouat**

**Faculty of Technology**

**Department of Electronics**

# MASTER THESIS

**DOMAINE:** Science & Technology

**OPTION:** Automation & Industrial Computing

**BOUCHENAK Halima** & **DIMEH Maria**

**Theme**

# Solar PV Emulator based Isolated Converter: Design & Simulation

**Jury members:**

| | | | |
|---|---|---|---|
| BELKHIRIE Mohammed | Pr | UATL | President |
| ABOUCHABANA Nabil | MCB | UATL | Examiner |
| HADJAISSA Aboubakeur | MCA | UATL | Supervisor |
| BENMILOUD Mohammed | MCB | UATL | Co-Supervisor |

**2023 / 2024**

# Abstract

*The photovoltaic emulators (PVE) aims to mimic the behavior of PV panels. The objective of this work is to design a photovoltaic emulator based on a DC-DC push-pull converter and ANN. The latter used to emulate a PV model in order to generate a current reference of PVE. Two control techniques were proposed to control PVE based ANN, the PID controller proposed as a first control strategy, and as second control strategy we proposed LQR controller. In addition, the add of the current observer, by using only a voltage sensor, make our proposed PVE more accurate, less expensive to produce, and more reliable than sensed signals. The results of the comparison between the PID and proposed LQR control strategy show the effectiveness of the LQR strategy in terms of steady state and response time of the PV panel emulator.*

**Keywords:** ***PV Emulator, Neural-Network, Push-Pull DC-DC Converter, PID, LQR.***

# ملخص

تهدف المحاكيات الكهروضوئية $(PVE)$ إلى محاكاة سلوك الألواح الكهروضوئية. الهدف من هذا العمل هو تصميم محاكي كهروضوئي يعتمد على محول الدفع والسحب $DC-DC$ والشبكة العصبية الاصطناعية $(ANN)$ . تم استخدام الأخيرة لمحاكاة نموذج $PV$ من أجل إنشاء مرجع تيار لـ $PVE$ .

تم اقتراح تقنيتين للتحكم للتحكم في $PVE$ المستندة إلى $ANN$ ، حيث تم اقتراح وحدة التحكم $PID$ كاستراتيجية التحكم الأولى، وكاستراتيجية التحكم الثانية اقترحنا وحدة التحكم $LQR$ .

بالإضافة إلى ذلك، فإن إضافة مراقب التيار، باستخدام مستشعر الجهد فقط، تجعل $PVE$ المقترح أكثر دقة وأقل تكلفة في الإنتاج وأكثر موثوقية من الإشارات المستشعرة.

توضح نتائج المقارنة بين استراتيجية التحكم $PID$ والاستراتيجية المقترحة $LQR$ فعالية استراتيجية $LQR$ من حيث الحالة المستقرة وزمن الاستجابة لمحاكي اللوحة الكهروضوئية.

# Resumé

Les émulateurs photovoltaïques (PVE) visent à imiter le comportement des panneaux solaires photovoltaïques. L'objectif de ce travail est de concevoir un émulateur photovoltaïque basé sur un convertisseur DC-DC à push-pull et un réseau de neurones artificiels (ANN). Ce dernier est utilisé pour émuler un modèle PV afin de générer une référence de courant pour le PVE.

Deux techniques de contrôle ont été proposées pour contrôler le PVE basé sur l'ANN : le contrôleur PID comme première stratégie de contrôle, et comme deuxième stratégie de contrôle, nous avons proposé le contrôleur LQR.

De plus, l'ajout d'un observateur de courant, en n'utilisant qu'un capteur de tension, rend notre PVE proposé plus précis, moins coûteux à produire et plus fiable que les signaux mesurés.

Les résultats de la comparaison entre la stratégie de contrôle PID et la stratégie de contrôle LQR proposée montrent l'efficacité de la stratégie LQR en termes d'état stationnaire et de temps de réponse de l'émulateur de panneau solaire photovoltaïque.
**Mots clés : PVE : Émulateur PV, Réseau de neurones, Convertisseur DC-DC push-pull, PI, LQR.**

# Acknowledgements

We would like to express our deepest gratitude to our advisor, Dr.HADJAISSA Aboubakeur, for his invaluable guidance, continuous support, and profound encouragement throughout the course of this research. His extensive knowledge and expertise have been fundamental to the successful completion of this work.

We extend our sincere thanks to our co-supervisor, Dr.BENMILOUD Mohammed, for his insightful feedback, constructive criticism, and unwavering support. His assistance has been pivotal in shaping the direction and quality of this research.

We also wish to acknowledge the members of our committee, Pr. BELKHIRIE Mohammed and Dr.ABOUCHABANA Nabil. Their thorough review, critical insights, and helpful suggestions have significantly contributed to the improvement of this study. Their expertise and dedication have been greatly appreciated.

Our heartfelt appreciation goes to our families for their endless support, understanding, and encouragement. Your love and patience have been a constant source of strength and motivation throughout this journey.Finally, We would also like to thank the teaching team and administrative body of the Faculty of Technology. Your dedication to education and your unwavering support have provided us with the resources and environment necessary to pursue and complete this research.

Thank you all for your mentorship, guidance, and support. This research would not have been possible without your contributions and encouragement.

# Contents

# List of Figures

# General Introduction

The quest for ever-better solar power systems hinges on precisely mimicking real-world conditions. This research tackles analyze and simulate photovoltaic (PV) emulators.

PV emulators, essentially electronic replicas of PV panels, are crucial tools for researchers. Real PV panels generate DC electricity influenced by sunlight intensity (irradiance), temperature, and other environmental factors. PV emulators replicate these characteristics by producing adjustable DC voltage and current outputs. This allows researchers to analyze how solar power systems would perform under various controlled conditions.

In general, photovoltaic emulators (PVEs) comprise three key components: power electronics (often a DC-DC converter) to manage power flow, a PV model mimicking real solar panel behavior and a control strategy to ensure accurate emulation.

The main objective of our project is to study and simulate the PV emulator system that consists of the PV model based electrical circuit and Neural Network Model, the control strategy (started by classical control PID and advanced LQR), and the power converter based on DC-DC Push-pull. Ading a current observer using only a voltage sensor enhances the accuracy, cost-effectiveness, and reliability of our proposed PVE compared to traditional sensing methods.

This study delves into using a DC-DC push-pull converter, a circuit adept at managing power flow, to simulate the emulator's setup. By simulating this setup, researchers can glean valuable insights into the emulator's functionality.

The incorporation of a neural network adds another dimension. Neural networks, inspired by the human brain, excel at learning intricate patterns from data. In this case, the neural network could be trained on real PV panel data to create even more realistic simulations for the PV emulator.

This project is structured around three chapters organized as follows:

• **The first chapter** dives into the world of PV generators, with a particular emphasis on how we can accurately mimic their behavior for testing purposes. We'll start by exploring the growing significance of PV power and the increasing need for reliable emulators to assess their performance.

The chapter will then unpack two key approaches for modeling PV behavior: electrical circuit models and neural networks. We'll then take dive into the various types of DC-DC converter circuits commonly used in PV systems.

• **The second chapter** dives deep into the push-pull converter, focusing on modeling and control using the state space representation approach. We'll also explore the design and analysis of a LQR and PID controller based on poles placements. The chapter kicks off with an introduction to the push-pull converter, explaining its operational modes and switching mechanisms. Next, analysis of a LQR and PID controller for the push-pull converter.Also, Our proposed photovoltaic energy (PV) system enhances by incorporating a current observer, by measuring PVE voltage only.

• **The last chapter** describes the design and validation of the photovoltaic (PV) emulator. It covers the emulator's function and its underlying electrical model.The chapter then discusses simulating the emulator's performance under various conditions. Finally, it validates the emulator's accuracy by comparing its output to real PV panels, focusing on key metrics like power output and response.

# Chapter 1

# An Overview on PV Emulators and DC-DC Converters

## 1.1 Introduction

Photovoltaic emulators replicate PV modules' behavior by mimicking their electrical characteristics, including voltage-current (V-I) curves. This emulation aids researchers, manufacturers, and engineers in evaluating system performance across diverse conditions, accurately replicating factors like solar irradiance and temperature. They offer a controllable power source through DC-DC converters, enabling simulation of various solar power levels and dynamics, with precise control over parameters like maximum power point tracking (MPPT) for optimal power extraction. These emulators find utility in testing and optimizing PV system components, algorithm development, grid integration studies, and educational purposes. Meanwhile, DC-DC converters manage power flow within PV systems, converting and controlling voltage and current levels between system components, thus facilitating efficient power transfer and integration with the electrical grid or other energy storage systems.

## 1.2 Necessity of PV Emulators

Testing and optimizing photovoltaic (PV) systems can be tricky. Real-world sunlight is notoriously fickle, making it challenging to replicate consistent conditions for thorough

analysis. This is where PV emulators step in PV panels are influenced by several factors, including the intensity of sunlight (irradiance), temperature, and construction materials. These factors all impact a panel's electrical output, measured by current and voltage (I-V characteristics).

A photovoltaic (PV) emulator replicates the current-voltage characteristics of real PV panels under diverse conditions, allowing detailed analysis and optimization of PV systems. It simulates various scenarios, including different irradiance levels and temperatures, enabling the study of their impact on a PV system's efficiency, reliability, and overall performance.

## 1.3 Photovoltaic Emulator design

A typical PV emulator comprises three fundamental components. The first is the PV model, which mathematically replicates the electrical behavior of a real PV panel. The second component is the control strategy, a critical element that directs the operation of the third component, the DC-DC converter. Figure 1.1 depicts these three foundational components of a PV emulator.

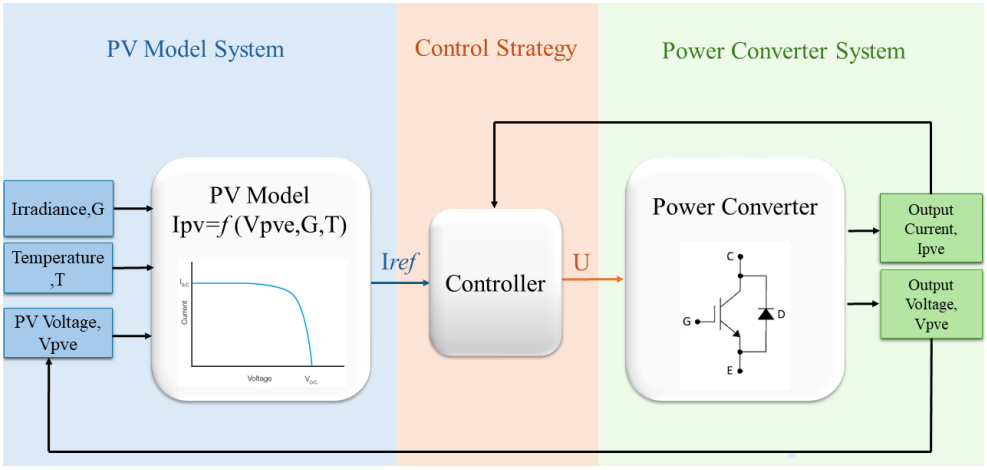


Figure 1.1: The three parts of the PV emulator system.

• **PV Model**: This generates a signal replicating the current-voltage (I-V) characteristics of a real PV panel. This is the foundation of the emulator, but for smooth operation, calculations must happen in real-time. Therefore, the model needs to be simplified while still accurately reflecting real-world I-V behavior [1].

• **Control Strategy**: This component bridges the PV model and the power converter by coordinating their operation to determine the emulator's operating point. An effective control strategy must accurately track the PV model's signal, provide stable emulator output, minimize computational demands, adapt to different PV modules without major changes, and avoid interfering with the power converter or load[1].

• **Power Converter**:

Power converters serve as essential components in electronic systems, meticulously adapting voltage and current levels to precisely meet the demands of connected loads[2].

## 1.4 Photovoltaic model

PV emulator design involves two model choices: the type of PV model and the implementation method within the controller. There are two main model types and five methods exist [1], as show in Figure 1.2:

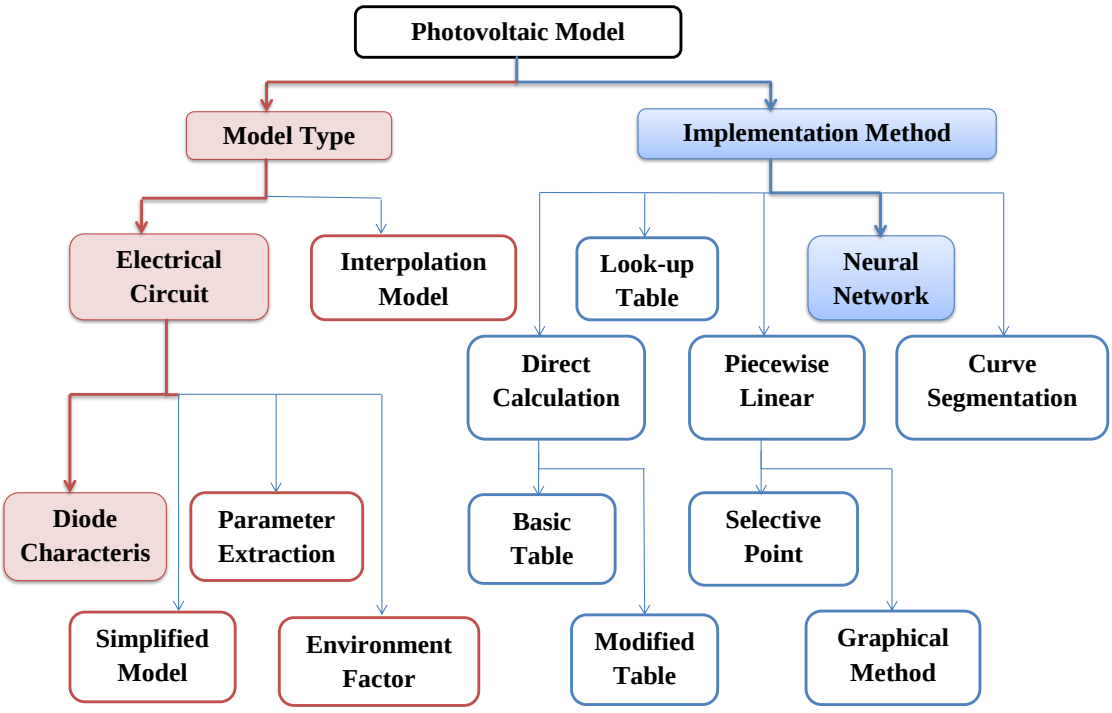


Figure 1.2: PV model overviews in the PV emulator application.

### 1.4.1 Electrical circuit model

PV emulators often use electrical circuit models to represent PV panels. These models, derived from circuit laws, are called analytical models. Two common types are the single diode model (1D2R) and the double diode model (2D2R). The single diode model is simpler and more accurate for emulator applications, while the double diode model, though more complex, is rarely used due to this trade-off [3]. in our study we focused only on the first type (The single diode model), Figures 1.3.

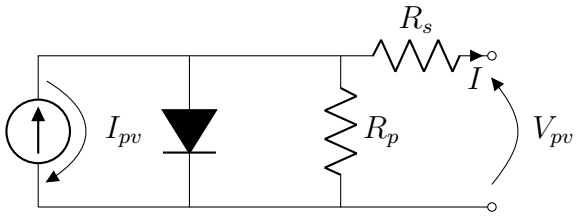


Figure 1.3: Circuit representation of the single diode model (1D2R Model).

#### Diode characteristics

Within photovoltaic (PV) modeling, an electrical circuit model offers a simplified representation of the PV system. This approach enables the derivation of the characteristic equation, which mathematically describes the relationship between voltage and current within the PV system, leveraging Kirchhoff's current law.[4]

the output equation of single diode is given as (Eq:1.1):

$$I = I_{pv} - I_s(e^{\frac{V_{pv}+IR_s}{AV_T}} - 1) - \frac{V_{pv} + IR_s}{R_p} \tag{1.1}$$

Where :

$I$: is the output current of the PV cell or module.

$V_{pv}$ : is the voltage across the PV cell or module.

$I_{pv}$: is the photo-current generated by the incident light.

$I_s$ : $are the reverse saturation current of the diodes.$

$R_s$ : is the series resistance.

$R_p$ : is the shunt resistance.

$A$ : are the diode ideality factors.

$V_T$ : is the thermal voltage

$$V_T = \frac{kT}{q}$$

Where:

$k$ : the Boltzmann constant ($1.38 \times 10^{-13} J/K$)

$T$ : the temperature in Kelvin

$q$: is the elementary charge ($1.6 \times 10^{-19} C$).

### 1.4.2 Artificial Neural network (ANN)

The implementation of the neural network PV model in the PV emulator is uncommon. In general, I-V characteristic data is obtained either from the experimental process[5] or the electrical circuit PV model[6] at different loads, irradiance and temperature. The data is trained offline before the neural network PV model is generated. The training process generates the PV hyper-surface in the current-voltage-irradiance-temperature working space. Since the working space is four dimensions, the number of neurons is carefully chosen. After the training process is completed, the neural network PV model is implemented inside the PV emulator system [1].

Artificial neural networks are used for tasks such as nonlinear modeling, pattern recognition and classification, and processing large volumes of data .This study specifically focuses on a type of ANN called a Multilayer Perceptron ($MLP$) for its ability to analyze large volumes of data for predictions [7] [8].

MLPs have a layered structure, typically containing[9]:

•**Input layer**: Receives the raw data.

•**Hidden layers (one or more)**: These layers process the data using non-linear activation functions. These functions essentially transform the data in a way that allows the network to learn complex patterns.

•**Output layer**: Provides the final prediction based on the processed data.

This study explores two specific activation functions for the hidden layers:

◦ Sigmoid function: Often used for tasks where the output represents a probability between 0 and 1.Eq (1.2).

◦ Linear function: Useful when the output can have any real value.Eq (1.3)

$$sigmoid(x)\frac{1}{1+e^{-x}} \tag{1.2}$$

$$Linear(z) = \lambda z \tag{1.3}$$

By employing nonlinear activation functions like the sigmoid function, neural networks can efficiently learn and represent intricate patterns, enabling them to tackle a wide range of challenging tasks. The linear function is a function where the output varies by a constant multiple of the input [7][9].

Many artificial neural networks rely on the Levenberg-Marquardt (LM) algorithm for learning and improvement. This algorithm tackles a specific challenge: optimizing performance in situations with non-linear relationships between inputs and outputs [7] [8].

LM helps the neural network adjust its internal connections (weights and biases) to minimize errors in its predictions.

$$y_i = f(\sum_j \omega_{ij}^{(k)} x_j + b_i^{(k)}) \tag{1.4}$$

Where $y_i$ is $ith$ the output layer,$\omega(k)$ $\omega_{ij}$ is the weight for the $ith$ neuron and the $jth$ input in the $kth$ hidden layer,$x_j$ is the $jth$ input to the neuron, and $b_i^{(k)}$ is the bias for the neuron in the $kth$ hidden layer.The $MLP$ network consists of an input layer, hidden layers,and an output layer[7].The output $h_i^{(k)}$ of the $ith$ neuron in the $kth$ hidden layer is computed as follows[10].

$$h_i^{(k)} = f(\sum_j \omega_{ij}^{(k)} h_j + b_i^{(k)}) \tag{1.5}$$

Where $h_i^{(k)}$ represents the output of the $jth$ neuron in the $kth$ hidden layer.Each hidden layer has a sigmoid activation function.The network's output can be written as

$$y_i = f(\sum_j \omega_{ij}^{(k)} h_j + b_i^{(k)}) \tag{1.6}$$

*MLP* has the structure of feeding the output of a hidden layer into the input vector of the next hidden layer or the output layer[7]. The input layer in this case consists of a three dimensional vector of voltage (V), irradiance (G) and temperature (T), and the output vector is a one dimensional vector of current (I). The structure of the artificial neural network is shown in Figure 1.4:

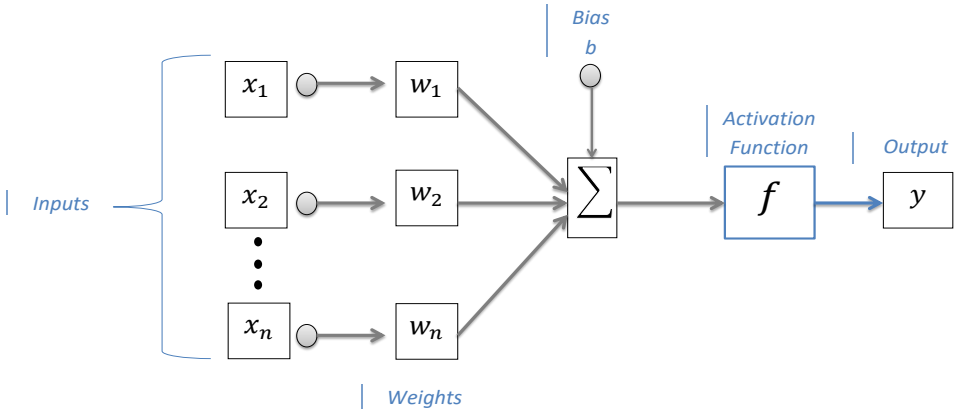


Figure 1.4: The structure of the artificial neural network

## 1.5 DC-DC Converter

Central to the operation of many electronic devices is the DC-DC converter. This critical circuit element functions by transforming a direct current (DC) voltage from one level to another. This capability is essential, as various components within a device may necessitate distinct voltage levels for proper operation [11].

DC-DC converters achieve this voltage transformation using switch-mode circuitry. Imagine tiny switches rapidly turning on and off, controlling the flow of current to manipulate the voltage level. This approach allows for highly efficient conversion, with some converters even reaching near-perfect 100% efficiency!.

Finally, DC-DC converters can be further categorized based on the current flow pattern within a critical component known as the inductor. Two primary operational modes exist in this context:

◦ Continuous conduction mode (CCM): In this mode, current always flows through the inductor, regardless of the switch state.

◦ Discontinuous conduction mode (DCM): Here, the current through the inductor can drop to zero during certain switch operations, briefly interrupting power flow in the circuit.[12]

### 1.5.1 Typologies of DC-DC Converter

DC-DC converters encompass a diverse range of electronic circuits, each meticulously designed to fulfill the unique voltage demands of direct current (DC) loads. These converters function as switching mode regulators, adeptly transforming an unregulated DC voltage into a precisely controlled level suitable for powering various device components[11].

Based on Figure 1.5 we can distinguish two different categories of DC-DC converter:

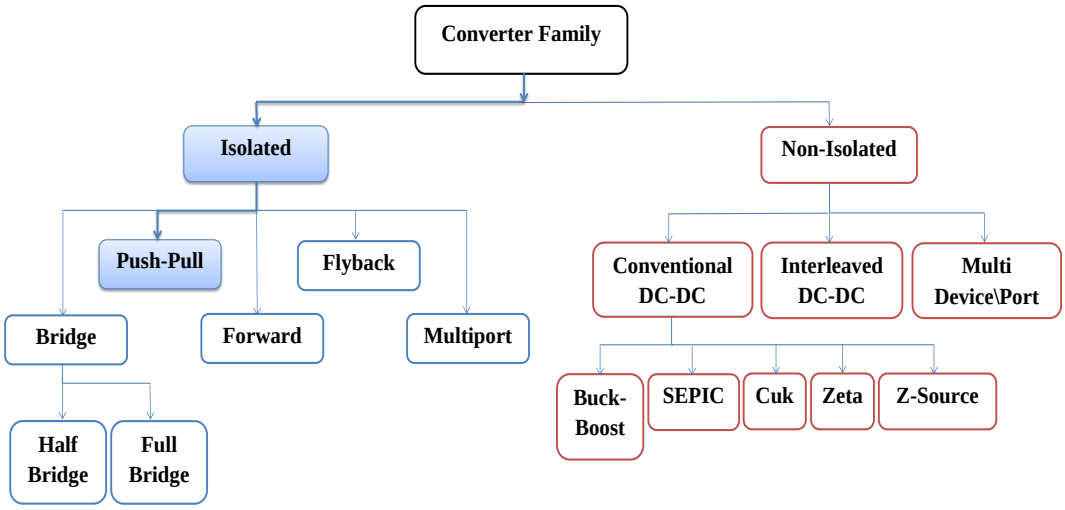


Figure 1.5: DC-DC Converter Family.

#### Isolated Converters

In practical applications the power supplies and power converters are designed and built to incorporate isolation between the input source side circuit and the output load side circuit as shown in Figure 1.6. Providing isolation has many benefits. Few of the important benefits are the following[13]:

1. Galvanic isolation between source side and load side, that is, no physical connection between source side and load side. This suppresses all common mode electro-

magnetic interference (EMI).

2. The turns ratio can be used as a fixed gain for achieving output voltage amplification or attenuation. This will give the designer more flexibility to choose the range of duty ratio.

3. With isolation, the converter can be designed to have multiple outputs each with different voltages and grounds[4].

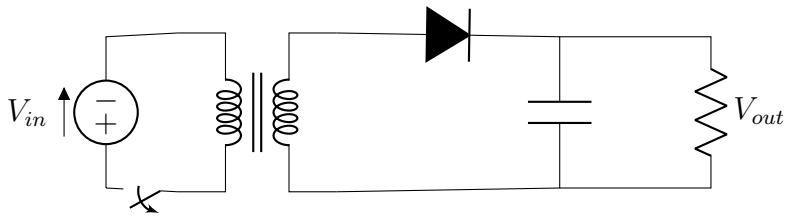


Figure 1.6: Typical isolated circuit diagram.

### Non-Isolated Converters

Non-isolated converters, as the name suggests, do not provide electrical isolation between the input and output circuits. The input and output share the same reference ground, and there is a direct electrical connection between them. Non-isolated converters are typically simpler and more cost-effective compared to isolated converters. They are commonly used in applications where isolation is not necessary or where the input and output share the same ground reference [14].

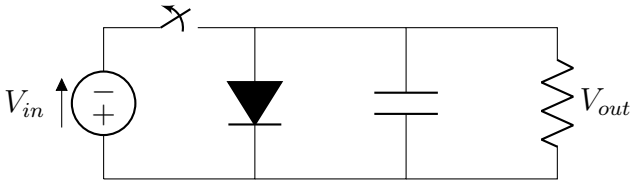


Figure 1.7: Typical Non-isolated circuit diagram.

Picking the right converter depends on what your project needs. Isolated converters provide a safety barrier, reduce electrical noise, and work with different voltage levels. Non-isolated converters are simpler and cheaper, making them a good choice when safety and noise aren't concerns [15].

## 1.6 Conclusion

This chapter explored the world of photovoltaic (PV) emulators and DC-DC converters. It highlighted the crucial role emulators play in simulating and rigorously testing PV systems, ensuring they perform at their best. The discussion delved into the different designs of DC-DC converters, showcasing their adaptability for various applications. Overall, the chapter emphasized the importance of PV emulators as a key technology in developing and testing solar energy solutions.

# Chapter 2

# Modeling and control of the Push-Pull Converter

## 2.1 Introduction

Push-pull converters excel at efficient $DC$ to $DC$ voltage conversion thanks to their clever transistor switching. To fine-tune this process, engineers can employ different control strategies that adjust signals based on errors.In literature, we can find lot of control techniques started by classical control and ended by advanced control.

In this chapter we will use two control techniques, the first one is PID and the second one is LQR, passing through modeling of push pull converter in order to do controller synthesis. Our proposed photovoltaic energy (PV) system enhances robustness by incorporating a current observer . so we need only to utilise a voltage sensor ,and can be integrated with LQR controller for even more precise power management in PV applications.

## 2.2 Push-pull Converter

The push-pull converter is a clever design for DC-DC converters, adept at efficiently transforming DC power between voltage levels. Its operation hinges on a simple principle: the alternate switching on and off of two switches[13].

The circuit diagram of the push pull converter as shown in Figure 2.1. It consists of:

Two mosfets ($Q1$ and $Q2$), Two diodes ($D1$ and $D2$), Transformer with a specific turns ratio ($N1 : N2$), Capacitor ($C$), Inductor ($L$), Input Voltage ($V_g$) , Output Voltage $V(t)$ and Load Resistance (R).

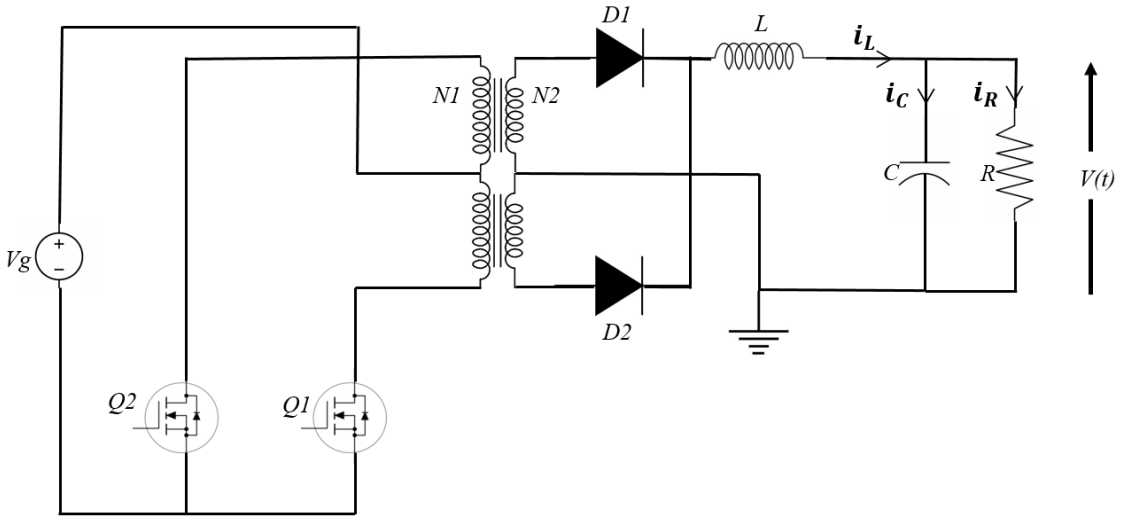


Figure 2.1: Circuit diagram of push–pull converter

### 2.2.1 Operation of push-pull Converter

The system utilizes two forward converters in an alternating fashion. Each converter delivers power to the load during a distinct half-cycle of the operating frequency.

#### Mode 1 (Q1 or Q2 is turned ON)

Q1 is on and $D1$ conducts; at the same time, the diode $D2$ is reverse biased and voltage across the filter inductor is positive and given as:

$$V_L = nV_g - V \tag{2.1}$$

Which forces $i_L$ through $D1$ to increase linearly.

With : $n = \frac{N_2}{N_1}$

the equivalent circuit of the converter is as in Figures (2.2 and 2.3)

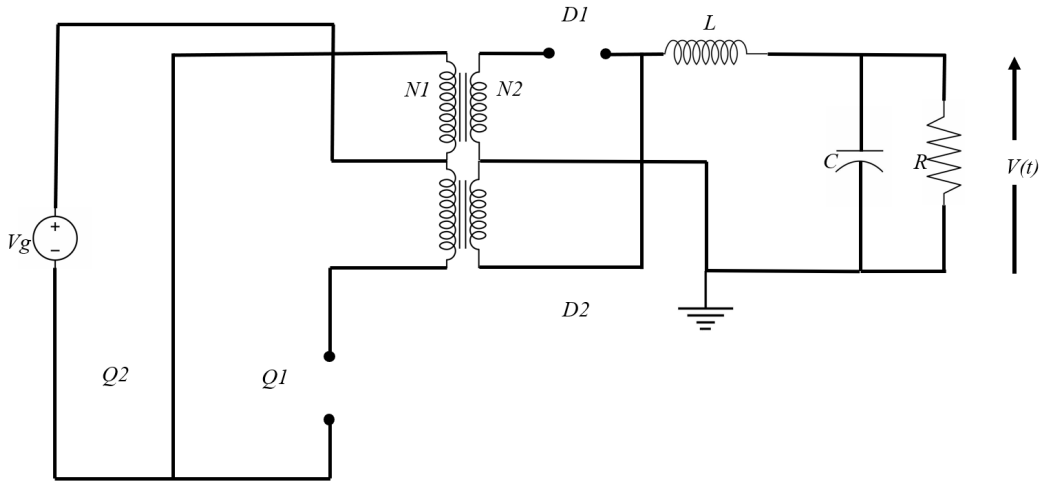


Figure 2.2: Circuit diagram When Q1 is ON and Q2 is OFF

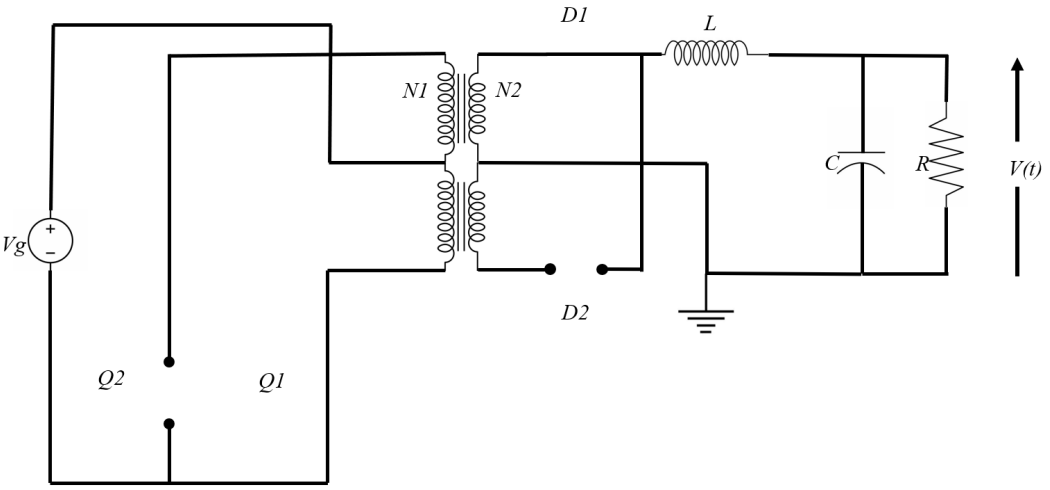


Figure 2.3: Circuit diagram when Q2 is ON and Q1 is OFF

**Mode 2 (Q1 and Q2 are turned OFF)**

when both switches are off as shown in Figure (2.4), the inductor current splits equally between the two secondary half-windings, which makes:

$$V_L = -V \tag{2.2}$$

$$i_{D1} = i_{D2} \tag{2.3}$$

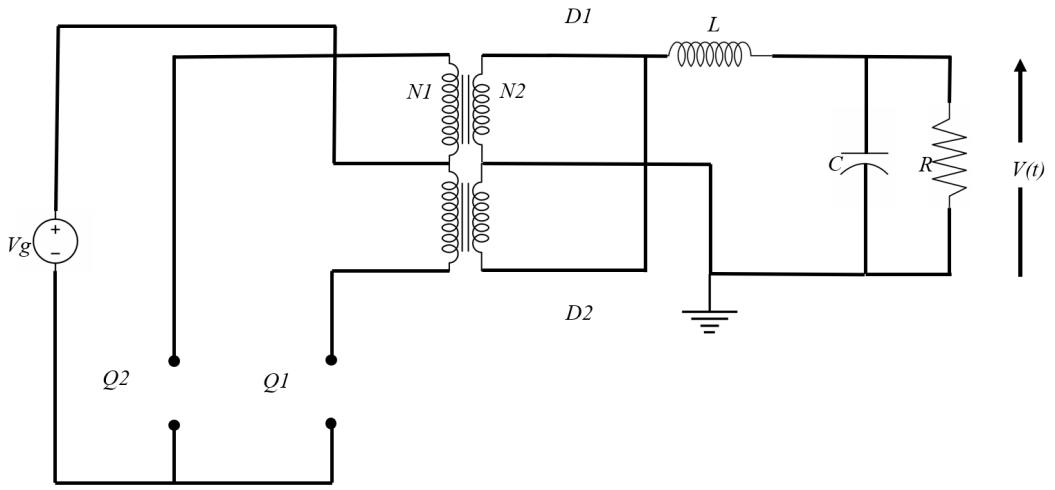


Figure 2.4: Circuit diagram when both Q1 and Q2 are OFF

### 2.2.2 Average Model of The Push-pull Converter

the dynamic model of the converter is represented by equations of the form[16]:

$$\dot{x} = Ax + Bu \tag{2.4}$$

$$y = Cx + Eu$$

A is state matrix,B is input matrix,C is output matrix,E is direct transition matrix,and x and y are input and output vector, respectively. The above equations are state and output equation of the model . The current flowing through the inductor ($i_L$) and voltage across the capacitor ($v_C$) is taken as state variables. The output voltage (V) and output current (I) are considered as output variables. The two distinct modes of operation in the converter for the purpose of modeling are:

- **Mode 1**: When one of the primary switches Q1 or Q2 is turned ON, the transfer of energy from primary to secondary circuit takes place and capacitor current increases. [4] For the duration dTs, the equivalent circuit of the converter is as in Fig 2.2

  Applying Kirchhoff's law at the dot across the inductance we find:

$$v_L + v_R = v_{N_2} \tag{2.5}$$

$$v_L = L\frac{di}{dt}, v_R = Ri_R \tag{2.6}$$

$$i_R = i_L - i_C \tag{2.7}$$

$$i_C = \frac{Ri_L}{Z_C + R} \Rightarrow Z_C i_C + Ri_C = Ri_L \tag{2.8}$$

$$Z_C i_C = v_C \Rightarrow v_C + Ri_C = Ri_L \tag{2.9}$$

$$i_C = i_L - \frac{v_C}{R} \tag{2.10}$$

$$v_C = \frac{1}{C}\int i_C dt \Rightarrow i_C = C\frac{dv_C}{dt} \tag{2.11}$$

$$\frac{Cdv_C}{dt} = -\frac{1}{R}v_C + i_L \tag{2.12}$$

Based on Eq(2.7) :

$$i_R = i_L - i_C \Rightarrow i_R = \frac{v_C}{R} \tag{2.13}$$

$$v_R = V \Rightarrow V = v_C \tag{2.14}$$

Based on Eq(2.5) :

$$v_L = v_{N_2} - V \tag{2.15}$$

$$v_{N_2} = \frac{N_2}{N_1}v_{N_1} \tag{2.16}$$

$$v_{N_1} = V_g \tag{2.17}$$

$$\frac{Ldi_L}{dt} = \frac{N_2}{N_1}V_g - v_c \tag{2.18}$$

The state equation and output equation are:

$$\begin{bmatrix} \frac{di_L}{dt} \\ \frac{dv_c}{dt} \end{bmatrix} = \begin{bmatrix} 0 & -\frac{1}{L} \\ \frac{1}{C} & -\frac{1}{RC} \end{bmatrix} \begin{bmatrix} i_L \\ v_c \end{bmatrix} + \begin{bmatrix} \frac{V_g}{L}\frac{N_2}{N_1} \\ 0 \end{bmatrix} \begin{bmatrix} u \end{bmatrix} \tag{2.19}$$

$$y = \begin{bmatrix} 0 & 1 \end{bmatrix} \begin{bmatrix} i_L \\ v_c \end{bmatrix} \tag{2.20}$$

- **Mode 2**: When both primary switches are turned off and energy stored in the inductor freewheels through secondary diodes.

  For the duration(1/2-d)Ts, the equivalent circuit of the converter is as in Fig 2.4

$$v_{N_2} = 0 \tag{2.21}$$

$$v_L + v_R = 0 \tag{2.22}$$

$$v_L = -v_R \tag{2.23}$$

$$\frac{Ldi_L}{dt} = v_c \tag{2.24}$$

$$\frac{Cdv_c}{dt} = i_L - \frac{1}{R}v_c \tag{2.25}$$

$$V = v_c \tag{2.26}$$

The state equation and output equation are:

$$\begin{bmatrix} \frac{di_L}{dt} \\ \frac{dv_c}{dt} \end{bmatrix} = \begin{bmatrix} 0 & -\frac{1}{L} \\ \frac{1}{C} & -\frac{1}{RC} \end{bmatrix} \begin{bmatrix} i_L \\ v_c \end{bmatrix} \tag{2.27}$$

$$y = \begin{bmatrix} 0 & 1 \end{bmatrix} \begin{bmatrix} i_L \\ v_c \end{bmatrix} \tag{2.28}$$

Similar modeling can be arrived when switch Q2 is ON and Q1 are OFF.Thus,the ON and OFF period of the converter is 2dTs and (1/2d)Ts, respectively. The average model of Mode 1 and Mode 2 are the same.The overall Matrix times the whole periode[17]:

$$AT = 2dTA_1 + 2TA_2(\frac{1}{2} - d) \Rightarrow A = A_2 \tag{2.29}$$

$$BT = 2dTB_1 + 2TB_2(\frac{1}{2} - d) \Rightarrow B = 2dB_1 \tag{2.30}$$

$$CT = 2dT(C_1 - C_2 + TC_2) \Rightarrow C = C_1 = C_2 \tag{2.31}$$

$$ET = 2dTE_1 + 2TE_2(\frac{1}{2} - d) \Rightarrow E = 0 \tag{2.32}$$

Thus,the averaged model of the push–pull converter is:

$$A = \begin{bmatrix} 0 & -\frac{1}{L} \\ \frac{1}{C} & -\frac{1}{RC} \end{bmatrix}, B = \begin{bmatrix} 2\frac{V_g}{L}\frac{N_2}{N_1} \\ 0 \end{bmatrix}, C = \begin{bmatrix} 0 & 1 \end{bmatrix}, E = \begin{bmatrix} 0 \end{bmatrix} \tag{2.33}$$

### 2.2.3 Transfer Functions

For the above small signal models, the transfer functions output Current to duty ($G_{i_d}(s)$) is obtained as :

$$G_{i_d}(s) = \frac{Y(s)}{U(s)} = C(sI - A)^{-1}B \tag{2.34}$$

$$Y(s) = I(s) \tag{2.35}$$

$$U(s) = d(s) \tag{2.36}$$

$$G_{i_d}(s) = \frac{I(s)}{d(s)} = \frac{2V_g\frac{N_2}{N_1}(sRC + 1)}{s^2LRC + sL + R} \tag{2.37}$$

For our work we used the following specification represented by the following tables 2.1 and 2.2:

| S.NO | Description | Value |
|---|---|---|
| 1 | Power output | 1.2 kW |
| 2 | Output voltage | 375 V |
| 3 | Switching frequency | 20 kHz |
| 4 | Maximum duty cycle | 0.5 |
| 5 | Converter efficiency (assumed) | 90 % |

Table 2.1: The specification of the Converter.

| S.NO | Component/parameter | Formula | Value |
|---|---|---|---|
| 1 | Input power | $P_{in} = \frac{P_{out}}{0.9}$ | 1.33 kW |
| 2 | Maximum average input current | $I_{in} = \frac{P_{in}}{V_{in}}$ | 33.33 A |
| 3 | Transformer turns ratio | $N = \frac{V_{out}}{2D_{min}V_{in}}$ | 12 |
| 4 | Maximum average output current | $I_{out} = \frac{P_{out}}{V_{out}}$ | 3.2 A |
| 5 | Filter inductor value | $L \geq (\frac{N_2}{N_1}V_{in} - V_{out})\frac{t_{on}}{\Delta I}$ | 570 mH |
| 6 | Output filter capacitor | $C = \frac{1}{8}\frac{\Delta I}{\Delta V}T$ | 1.6 uF |

Table 2.2: Component/parameter values

## 2.3 PID Controller

In a power electronic system, there's a crucial component called a controller that acts as the brain of the operation. Its job is to maintain a specific parameter, like output voltage and current or input current voltage, at a desired set point. The controller constantly monitors this parameter using sensors. It then compares the measured value to a predetermined reference value, like a set voltage level. Any difference between these two values is called the error signal. This error signal is essentially the controller's input. Based on the magnitude and direction (positive or negative) of this error, the controller generates a control signal.

In this specific case , a service turn (a control mechanism) is used to adjust the controller input. This adjustment typically involves converting a voltage level into a time value. This time value then becomes the controller's input, ultimately influencing the output voltage,to meet the required performance of stability, speed and accuracy

PID controller is designed to ensure that the error signal eventually reaches zero in steady-state conditions. This means the output current will precisely match the reference current over time.

To design a PID controller for the given transfer function using the pole placement method, we need to calculate $K_p$,$K_i$ and $K_d$.

The transfer function of push pull converter is given as :

$$G(s) = \frac{I(s)}{d(s)} = \frac{K(sRC+1)}{s^2LRC + sL + R} \tag{2.38}$$

Where : $K = 2V_g\frac{N_2}{N_1}$

Let's assume the desired closed-loop poles are $p_1$ , $p_2$ and $p_3$. The corresponding characteristic polynomial is:

$$P(s) = (s-p_1)(s-p_2)(s-p_3) = s^3 - s^2\alpha + s\beta - \gamma \tag{2.39}$$

Where :

$\alpha = p_1 + p_2 + p_3$

$\beta = p_1p_2 + p_1p_3 + p_2p_3$

$\gamma = p_1p_2p_3$

The transfer function of the system with a PID controller is:

$$C(s) = K_p + \frac{K_i}{s} + K_d s \tag{2.40}$$

The closed-loop transfer function is:

$$G_c(s) = \frac{G(s)C(s)}{1 + G(s)C(s)} \tag{2.41}$$

$$G_c(s) = \frac{s\frac{K(sRC+1)}{s^2LRC+sL+R}(K_p + \frac{K_i}{s} + K_d s)}{s(1 + \frac{K(sRC+1)}{s^2LRC+sL+R}(K_p + \frac{K_i}{s} + K_d s))} \tag{2.42}$$

$$G_c(s) = \frac{sK(sRC+1)(K_p + \frac{K_i}{s} + K_d s)}{s^3LRC + s^2L + R + K(sRC+1)(sK_p + K_i + s^2K_d)} \tag{2.43}$$

$$G_c(s) = \frac{sK(sRC+1)(K_p + \frac{K_i}{s} + K_d s)}{s^3 + s^2(\frac{L+KK_pRC+KK_d}{LRC+KK_dRC}) + s(\frac{R+KK_p+KK_iRC}{LRC+KK_dRC}) + \frac{KK_i}{LRC+KK_dRC}} \tag{2.44}$$

The closed-loop characteristic equation is:

$$D(s) = s^3 + s^2(\frac{L + KK_pRC + KK_d}{LRC + KK_dRC}) + s(\frac{R + KK_p + KK_iRC}{LRC + KK_dRC}) + \frac{KK_i}{LRC + KK_dRC} \tag{2.45}$$

Match this polynomial to the desired characteristic polynomial

$$P(s) = (s - p_1)(s - p_2)(s - p_3) = s^3 - s_2\alpha + s\beta + \gamma$$

- $s^2$ term : $\frac{L+KK_pRC+KK_d}{LRC+KK_dRC} = -\alpha$
- $s$ term : $\frac{R+KK_p+KK_iRC}{LRC+KK_dRC} = \beta$
- constant term : $\frac{KK_i}{LRC+KK_dRC} = -\gamma$

From the constant term equation:

$$K_i = -\gamma\frac{LRC}{K} + \gamma K_d RC \tag{2.46}$$

From the $s$ term equation with Substitute$K_i$:

$$K_p = -\frac{\beta LRC + \beta KK_dRC + \gamma L(RC)^2 + \gamma KK_d(RC)^2 - R}{K} \tag{2.47}$$

From the $s^2$ term equation with Substitute $K_p$:

$$K_d = \frac{L + (\beta LRC + \beta KK_dRC + \gamma L(RC)^2 + \gamma KK_d(RC)^2 - R)RC + KK_d}{LRC + KK_dRC} = -\alpha \tag{2.48}$$

After solving the simplified equations the values of $K_i$ , $K_p$ , and $K_d$ in terms of the given parameters $L$,$R$,$C$,$\alpha$,$\beta$, and $\gamma$ are:

$$K_p = -\frac{R(RC\alpha + 1)}{K((RC)^3\gamma + (RC)^2\beta + RC\alpha + 1)} \tag{2.49}$$

$$K_i = \frac{R(RC)^2\gamma}{K((RC)^3\gamma + (RC)^2\beta + RC\alpha + 1)} \tag{2.50}$$

$$K_d = \frac{-L((RC)^3\gamma + (RC)^2\beta + RC\alpha) + R(RC) - L}{K((RC)^3\gamma + (RC)^2\beta + RC\alpha + 1)} \tag{2.51}$$

We have :

$\alpha = p_1 + p_2 + p_3$

$\beta = p_1p_2 + p_1p_3 + p_2p_3$

$\gamma = p_1p_2p_3$

For our work we used the following specification :

$$\begin{cases} p_1 = 14 \\ p_2 = -14 + 10i \\ p_3 = -14 - 10i \end{cases} \Rightarrow \begin{cases} \alpha = -14 \\ \beta = -96 \\ \gamma = 4144 \end{cases} \Rightarrow \begin{cases} K_p = 60 \\ K_i = 2 \\ K_d = -6.6 \times 10^{-4} \end{cases} \tag{2.52}$$

## 2.4 LQR with Integral Action (LQI)

An LQI controller builds upon the LQR concept by adding an integrator. This makes LQI suitable for servo systems, where the goal is to track a specific non-zero reference point. LQI leverages optimal control theory, enabling it to track reference signals and reject disturbances[18].

Fig 2.5 illustrates the LQI controller's block diagram. This diagram includes matrices $A$, $B$, $C$ and $D$ representing the mathematical model of the plant under control. Additionally, $K$ represents the controller gain, and $K_i$ signifies the integrator gain.

r in our case is a reference of PV model ($I_{ref}$), (see Fig 1.1).

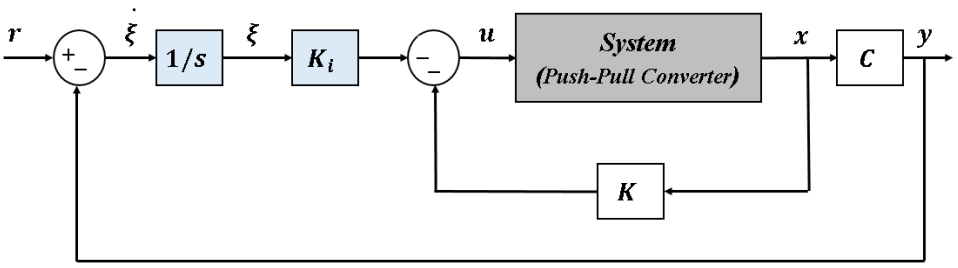


Figure 2.5: Block diagram of LQI controller

The state and output equations system can be written as follows:

$$\begin{cases} \dot{x} = Ax + Bu \\ y = Cx + Du \end{cases} \tag{2.53}$$

The conventional LQR design problem is to minimize the following quadratic performance index Eq(2.54) [19], balancing system performance (settling time, stability) with control effort [20].

$$J = \frac{1}{2}\int_0^{\infty} (X^T Q X + U^T R U)dt \tag{2.54}$$

The LQR design method seeks to determine a feedback gain matrix (K) that minimizes a pre-defined quadratic performance index. This minimization process aims to achieve a balance between three key factors:Control effort,Response magnitude and Response speed that will guarantee a stable system . By minimizing this function, the design process aims to find the optimal gain matrix (K) for the control vector [20] [21].

The linear optimal control input for LQR with integral action is:

$$u = -Kx - K_i\xi \tag{2.55}$$

where: $K = R^{-1}\hat{B}^T P$

The control law indicated in Eq(2.55) minimizes the performance index stated in Eq(2.54) where $x$ is an n-dimensional state-space vector, $u$ is an m-dimensional control input vector, $y$ is a p-dimensional output vector, $R \in \Re^{m\times m}$ is the square positive definite matrix and $Q \in \Re^{n\times n}$ is a positive semi-definite matrix, $\xi(t)$ is a new state due to adding integral action, $K$ is the LQR gain and $K_i$ is the integrator gain, and $P$ is the solution of matrix differential Riccati equation Eq(2.59) [20].

Substituting Eq(2.55) in Eq(2.59) yields,

$$\dot{x} = Ax + B(-Kx + K_i\xi) = (A - BK)x + (BK_i)\xi \tag{2.56}$$

$$\dot{\xi} = r - y = r - Cx \tag{2.57}$$

In the control of the Push Pull converter, the state variables used

$$x = \begin{bmatrix} x_1 & x_2 \end{bmatrix}^T = \begin{bmatrix} i_L & v_c \end{bmatrix}^T$$

With the addition of the integral action, an additional state is introduced, which is the error $\xi$. As a result, the matrices $A$, $B$, and $C$ of the plant to be controlled become[22]:

$$\begin{bmatrix} \dot{x} \\ \dot{\xi} \end{bmatrix} = \begin{bmatrix} A - BK & BK_i \\ -C & 0 \end{bmatrix} \begin{bmatrix} x \\ \xi \end{bmatrix} + \begin{bmatrix} B \\ 0 \end{bmatrix} u + \begin{bmatrix} 0 \\ I \end{bmatrix} r \tag{2.58}$$

The matrix algebraic Riccati equation is represented as follows [23]

$$PA + A^T P - PBR^{-1}B^T P + Q = 0 \tag{2.59}$$

The solution to the matrix Riccati equation for LQR control is guaranteed to be unique, symmetric, and positive semi-definite. This property ensures a well-defined and stable controller design. However, the performance of the LQR controller hinges critically on the selection of the weighting matrices,State weighting matrix $Q$ and Control weighting matrix $R$ [24].

The selection of $Q$ and $R$ plays a pivotal role in shaping the LQR controller's behavior and overall system performance. Therefore, employing an intelligent optimization method to determine these weighting matrices can significantly enhance the effectiveness of the LQR control design [20].

$$Q = \begin{bmatrix} i_L & 0 & 0 \\ 0 & v_c & 0 \\ 0 & 0 & \int I_{ref} - i_c \end{bmatrix}$$

For our work we used the following specification :

$$Q = \begin{bmatrix} 1 & 0 & 0 \\ 0 & 0 & 0 \\ 0 & 0 & 1e6 \end{bmatrix}, R = 1$$

### 2.4.1 Current Observer

As is usually the case, not all state variables can be directly measurable. we need to use a state observer [22]. In this work we proposed the add of a current observer to estimate the PVE current by measuring Voltage PVE. Figure 2.6 shows a block diagram of a type 1 servo system with a state observer.

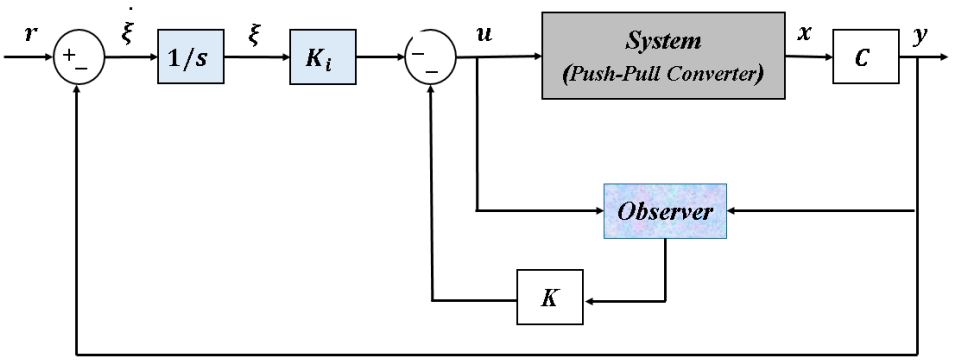


Figure 2.6: Type 1 servo system with state observer.

The observer is a subsystem to reconstruct the state vector of the plant. The mathematical model of the observer is basically the same as that of the plant, except that we include an additional term that includes the estimation error to compensate for inaccuracies in matrices $A$ and $B$ and the lack of the initial error[22]. The estimation error or observation error is the difference between the measured output and the estimated output Eq(2.62).The initial error is the difference between the initial state and the initial estimated state Eq(2.64).

Thus, we define the mathematical model of the observer to be

$$\dot{\widetilde{x}} = A\widetilde{x} + Bu + L(y - C\widetilde{x}) \tag{2.60}$$

$$\dot{\widetilde{x}} = (A - LC)\widetilde{x} + Bu + Ly \tag{2.61}$$

where $\widetilde{x}$ is the estimated state and $C\widetilde{x}$ is the estimated output.The inputs to the observer are the output $y$ and the control input $u$. Matrix $L$, which is called the observer gain matrix, is a weighting matrix to the correction term involving the difference between the measured output $y$ and the estimated output $C\widetilde{x}$.This term continuously corrects the model output and improves the performance of the observer. Figure 2.7 shows the full-order state observer [22].

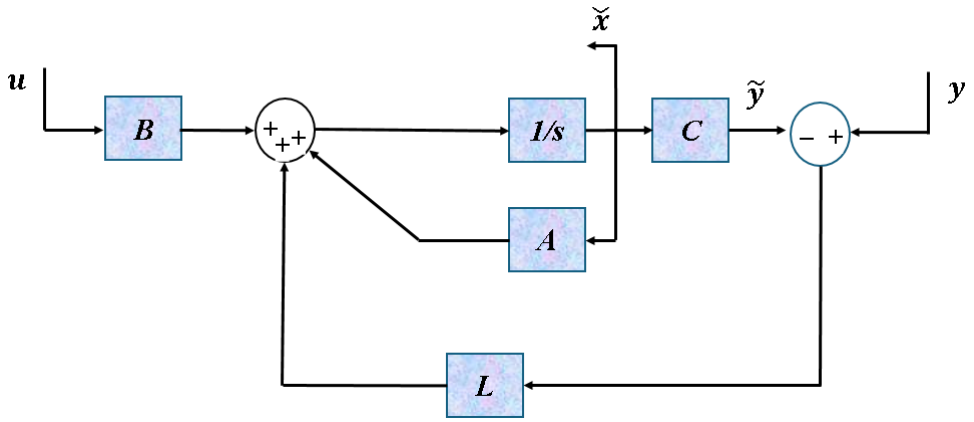


Figure 2.7: Full-order state observer

To obtain the observer error equation, let us subtract Eq(**??**) from Eq(2.53):

$$\dot{e} = \dot{x} - \dot{\widetilde{x}} = Ax - A\widetilde{x} - L(Cx - C\widetilde{x}) \tag{2.62}$$

$$\dot{e} = (A - LC)(x - \widetilde{x}) \tag{2.63}$$

Define the difference between $x$ and $\widetilde{x}$ as the error vector $e$, or

$$e = x - \widetilde{x} \tag{2.64}$$

Then Eq(2.65) becomes

$$\dot{e} = (A - LC)e \tag{2.65}$$

The dynamics of the whole system is obtained by combining the equations for $\dot{x}$ and $\dot{e}$

$$\begin{bmatrix} \dot{x} \\ \dot{e} \end{bmatrix} = \begin{bmatrix} A - BK & BK \\ 0 & A - LC \end{bmatrix} \begin{bmatrix} x \\ e \end{bmatrix} + \begin{bmatrix} B \\ 0 \end{bmatrix} r \tag{2.66}$$

$$y = \begin{bmatrix} C & 0 \end{bmatrix} \begin{bmatrix} x \\ e \end{bmatrix} \tag{2.67}$$

## 2.5 Conclusion

In this chapter we modeled the Push-Pull converter using state-space approaches, the latter explored in order to analyze and design two types of controllers PID and LQR.

The parameters of PID controller founded by the placement poles method.

# Chapter 3

# Simulation And Validation Of PV Emulator

## 3.1 Introduction

A photovoltaic (PV) emulator is a controllable power supply that mimics the electrical behavior of a solar panel but isn't influenced by external factors like temperature and irradiation.

This chapter is organised as follow:

− Validation of PV ANN model with PV electrical model.

−The push-pull converter tested in open loop and close loop by (PI, LQR and Observer).

− Simulation and validation of the photovoltaic emulator using Matlab/Simulink environment, our simulation will encompass various tests, including irradiance, temperature and load.

## 3.2 PV Emulator Functionality

Figure 3.1 presents a diagram block of photovoltaic emulator based on a push-pull converter and ANN, The design utilizes a Push-Pull converter for several reasons such as high efficiency, galvanic isolation between input and output, a wide range of compatible input voltages, low output ripple, and the ability to operate in both step-up and step-

down modes. a closed-loop control strategy regulates the duty cycle of the Push-Pull converter switch. This strategy compares the reference current derived from the PV Neural Network with the actual current feedback from the converter. The resulting error signal ($e$) is then fed to the controller to adjust the duty cycle and achieve the desired output.

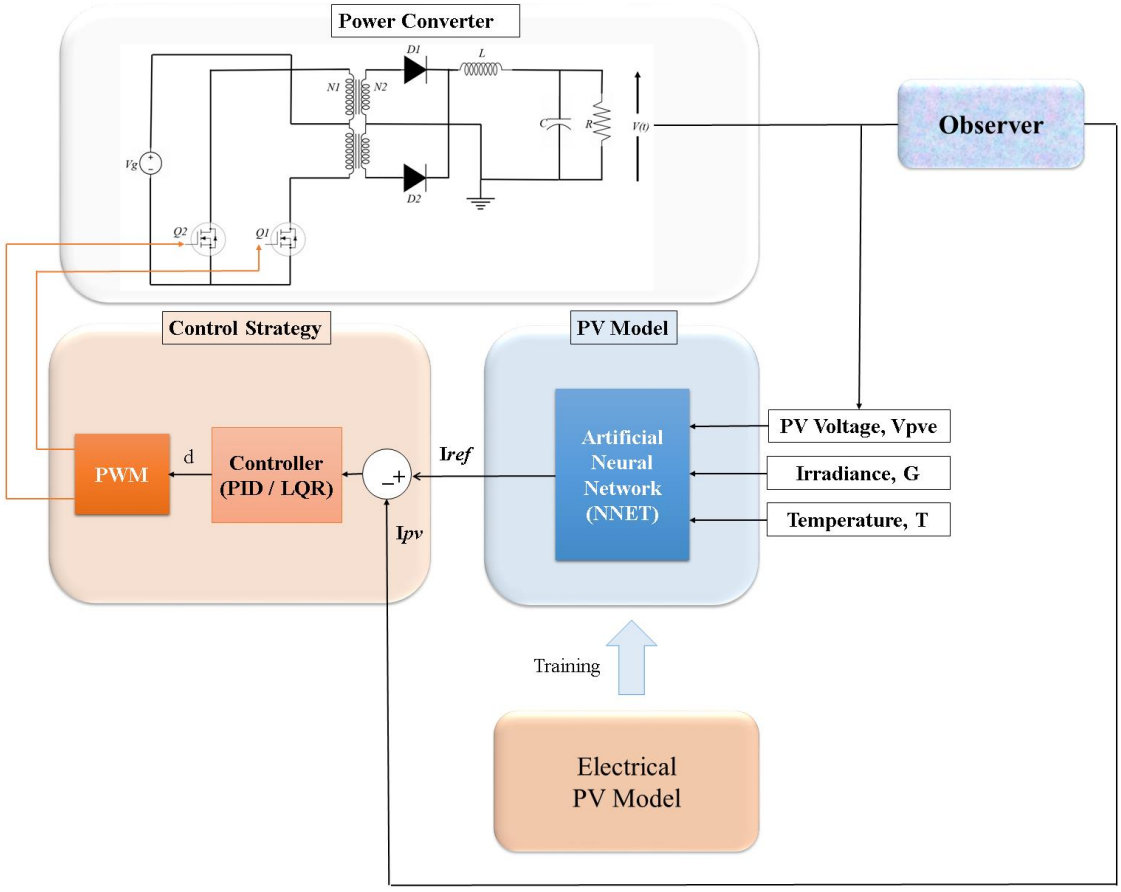


Figure 3.1: Block diagram of the PVE

## 3.3 ANN PV model

As we know, the ANN model needs data set informations Fig 3.2.


Figure 3.2: ANN PV model

in our work we used the electrical PV model Fig 3.3 (a) in order to generate a data set for training and creating an ANN PV model Fig 3.3 (b).

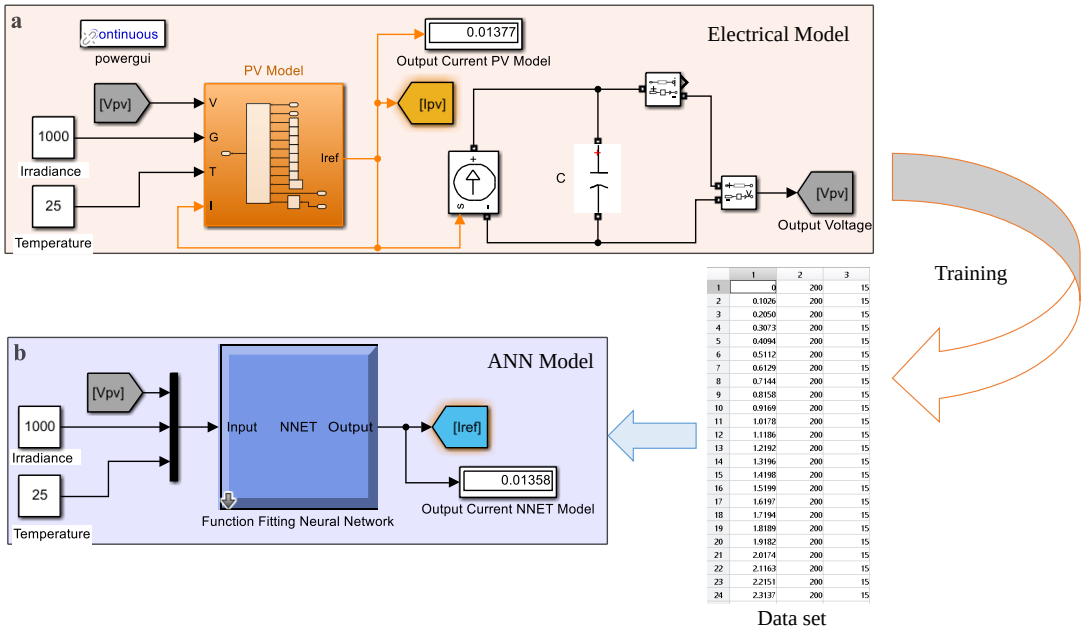


Figure 3.3: PV & ANN Model

The artificial neural network formed by three inputs (G,T,V) and one output witch is the current.

The settings for training the neural network for input are as follows: the maximum number of training epochs is 1000; the performance goal is $1 \times 10^{-9}$; and the learning rate is 0.05.

The regression analysis results in Figure 3.4, the data represent the actual value, while the fitting represents the predicted values. From scatter plot analysis perspective, we see that scatter points are distributed around the regression line. Secondly, slope of the line is close to 1,suggesting a strong positive relationship between the variables that the model effectively captures. Finally, from an error analysis perspective, the difference between the data and the fitting remains relatively constant.

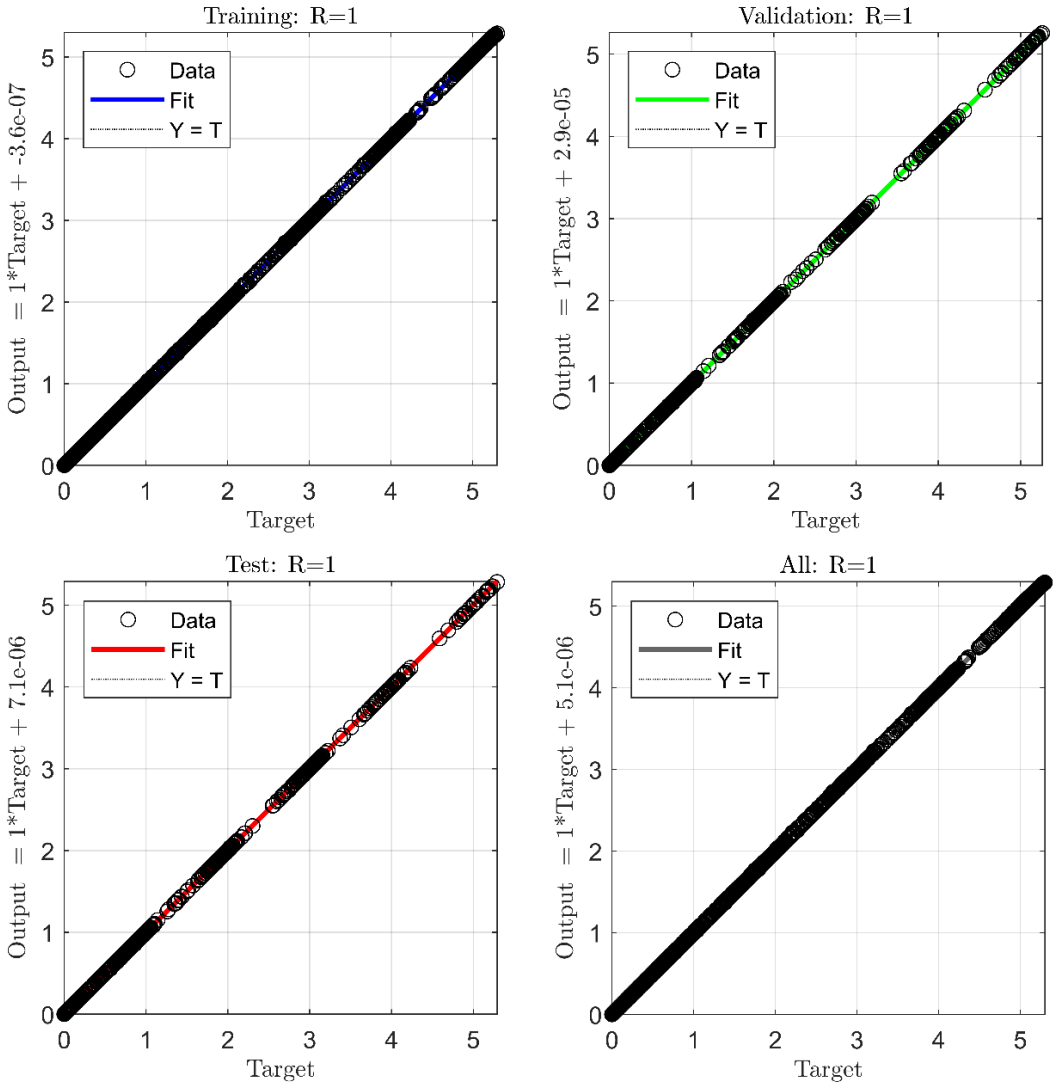


Figure 3.4: The Regression Analysis Result

In order to validate the founded ANN PV model , on successive simulations under Matlab/Simulink environment were explored under different conditions (T,G and Load).

### 3.3.1 Validation Of PV-Neural Network Model

In this section, we compared the electrical PV model to the neural network PV model. In this simulation we variate the load (capacitor) and we fixed (T and G). Figure 3.5 shows the compatibility rate between two PV Models so that the Error almost equal zero.

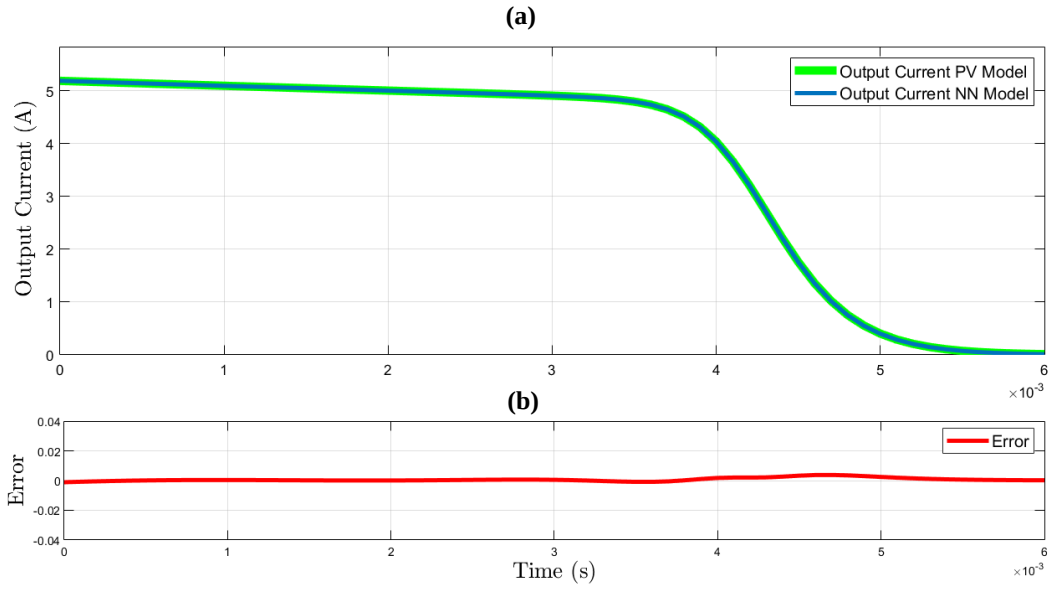


Figure 3.5: Output Currents & Error Between PV & ANN Model

From Figure 3.5.(a) one can see the exactness of two outputs current PV, electrical PV model and ANN-PV model , in this simulation the current changes from 5.2A which is $I_{sh}$ to 0A $V_{oc}$. while the second curve Figure 3.5.(b) shows the error between two models.

A PV panel's output power depends heavily on weather conditions, particularly solar radiation and temperature. While increased radiation proportionally boosts the short-circuit current, the open-circuit voltage remains fairly constant. Temperature has a lesser impact, but it causes a slight current rise and a decrease in voltage. illustrate the effects on electrical PV model through their I-V and P-V curves and The training data were compared with PV model under standard conditions As shown Figure 3.6 and 3.7.

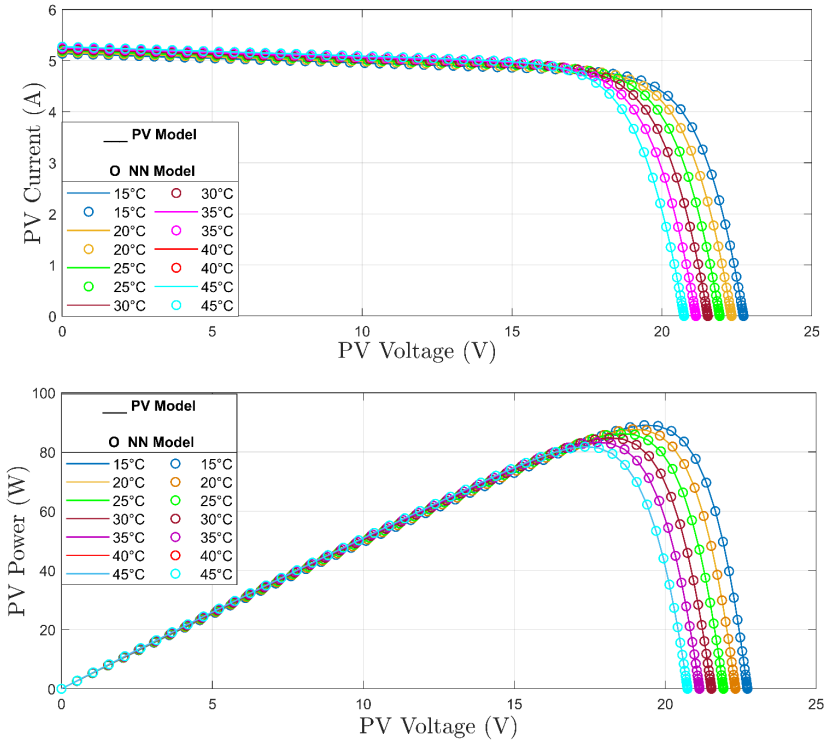


Figure 3.6: I-V and P-V curves under Temperature effects.

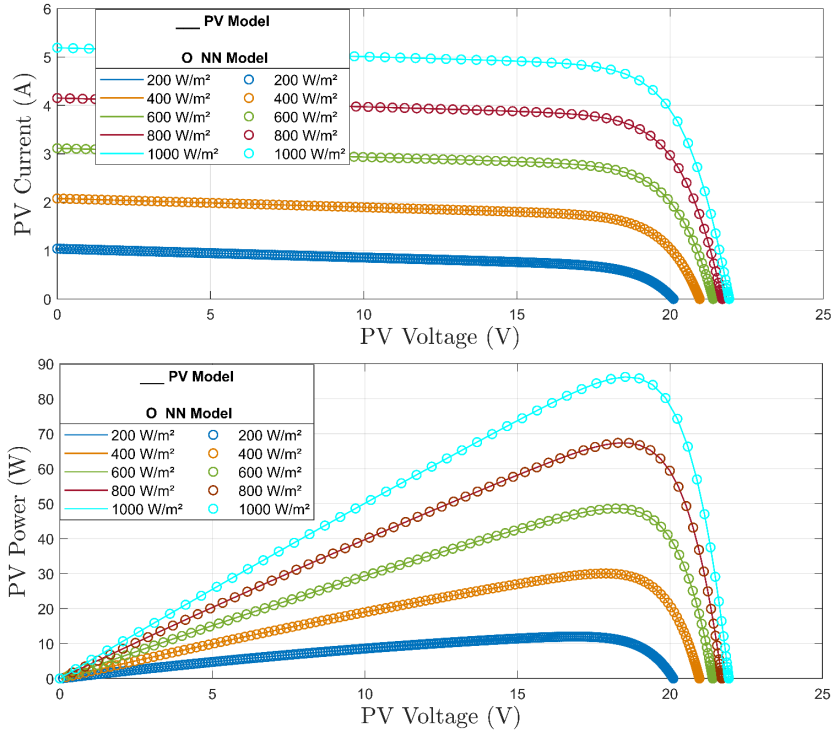


Figure 3.7: I-V and P-V curves under radiation effects.

The figure 3.6 shows the I-V and P-V curves of Solar-World panel (see Appendix 1) under temperature variation. We can see the matching of two models electrical and ANN-Model (cycls). The same thing in the curves of irradiance variation Figure 3.7.

## 3.4 Control of DC-DC Push-Pull Converter

In order to control a push-pull converter two test are made, open loop and closed loop(PID,LQR and Observer).

### 3.4.1 Open Loop Control

Figure 3.8 shows a push-pull converter controlled in open loop. In an open-loop configuration, the converter operates without feedback control. The switches are controlled with a fixed duty cycle ($\alpha$), typically generated by a pulse-width modulation (PWM) signal.

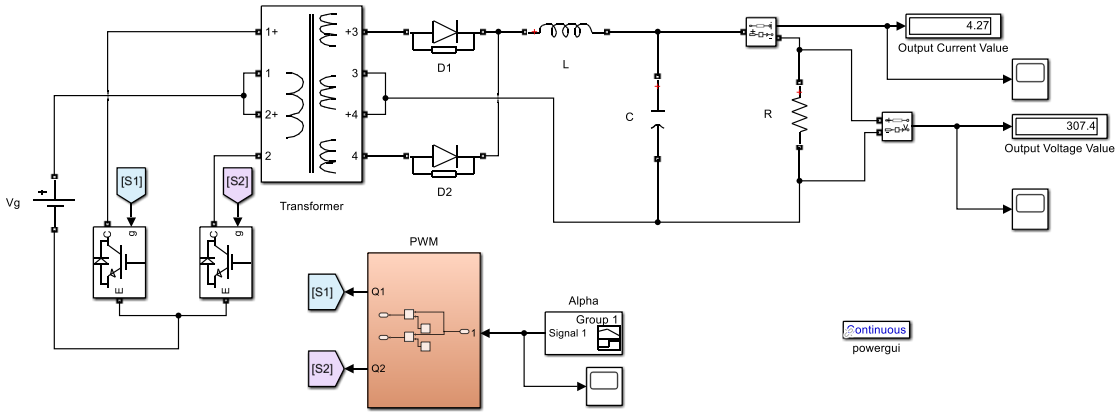


Figure 3.8: Push-pull converter in open loop

To test the Push-Pull DC-DC converter in open loop, three values of duty cycle Figure 3.9.(a) are tested . From curves Figures 3.9.(b) and 3.9.(c) we can see the output voltage and current of Push-Pull DC-DC converter , one can see steady state and response time are very acceptable for our application.

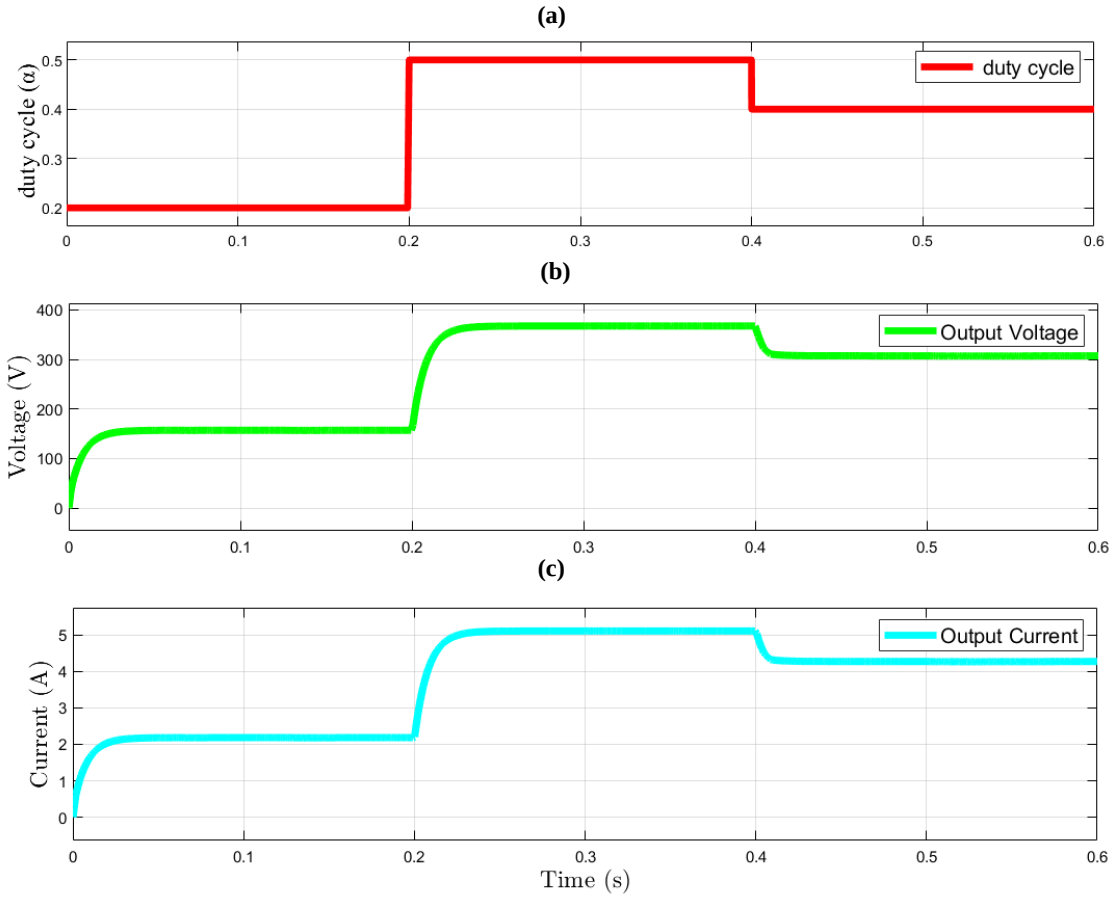


Figure 3.9: Push-Pull DC-DC curves in open loop

### 3.4.2 Close Loop Control

This section presents push pull converter controlled by two control strategies PID and LQR.

#### PID Controller

A Simulink model of the push-pull converter controlled by PID controller is presented in Figure 3.10 .

As we say in section 2.3 the PID parameters are founded using placement pole method.

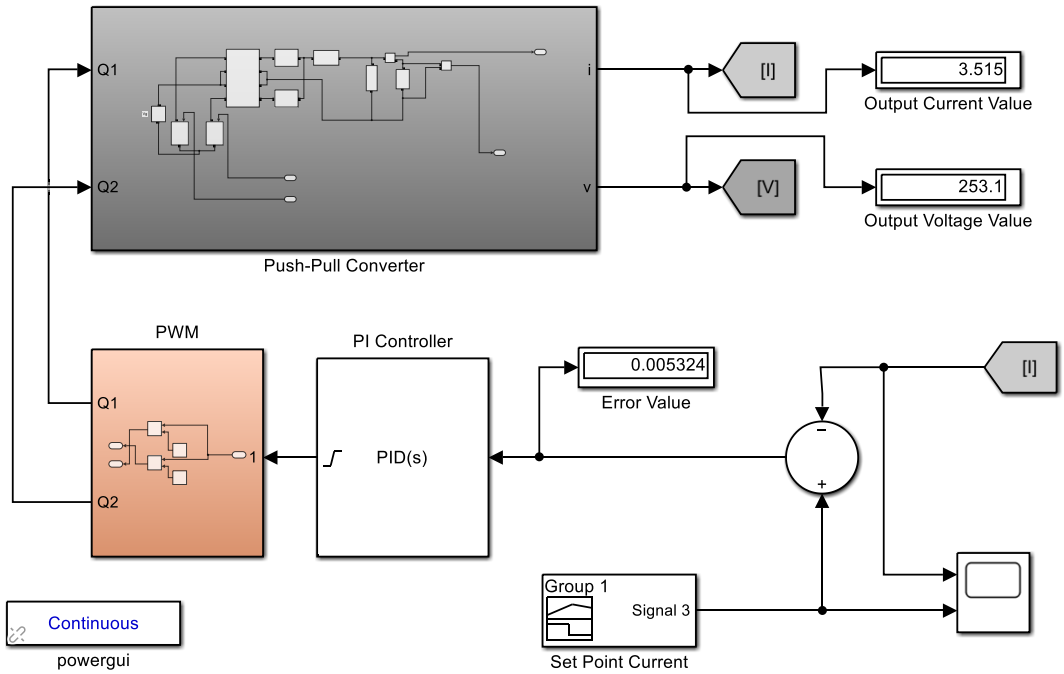


Figure 3.10: Push-Pull DC-DC converter with PID controller

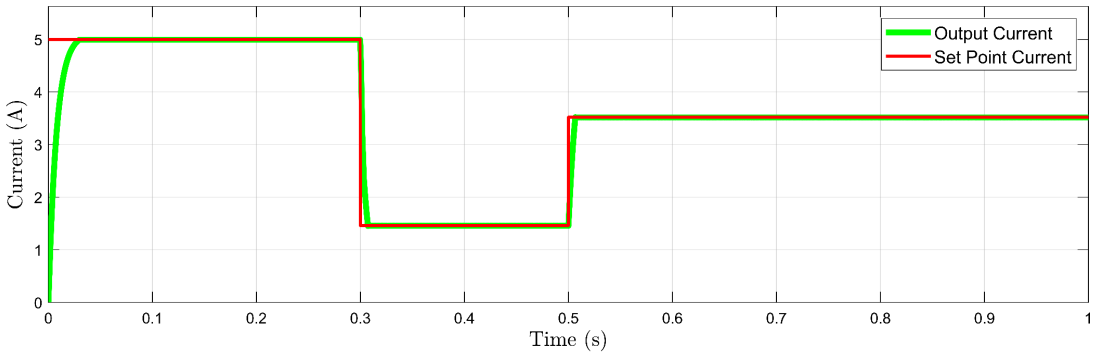


Figure 3.11: Push-Pull curves in close loop (PID controller)

In Figure 3.11, when the set point current is changed, the output current follows its reference. Additionally, the PID controller demonstrates its effectiveness in terms of response time and steady state when the set point changes abruptly.

### LQR Controller

A push-pull converter controlled with Linear Quadratic Regulator with Integrator action (LQI) control present an Figure 3.12.

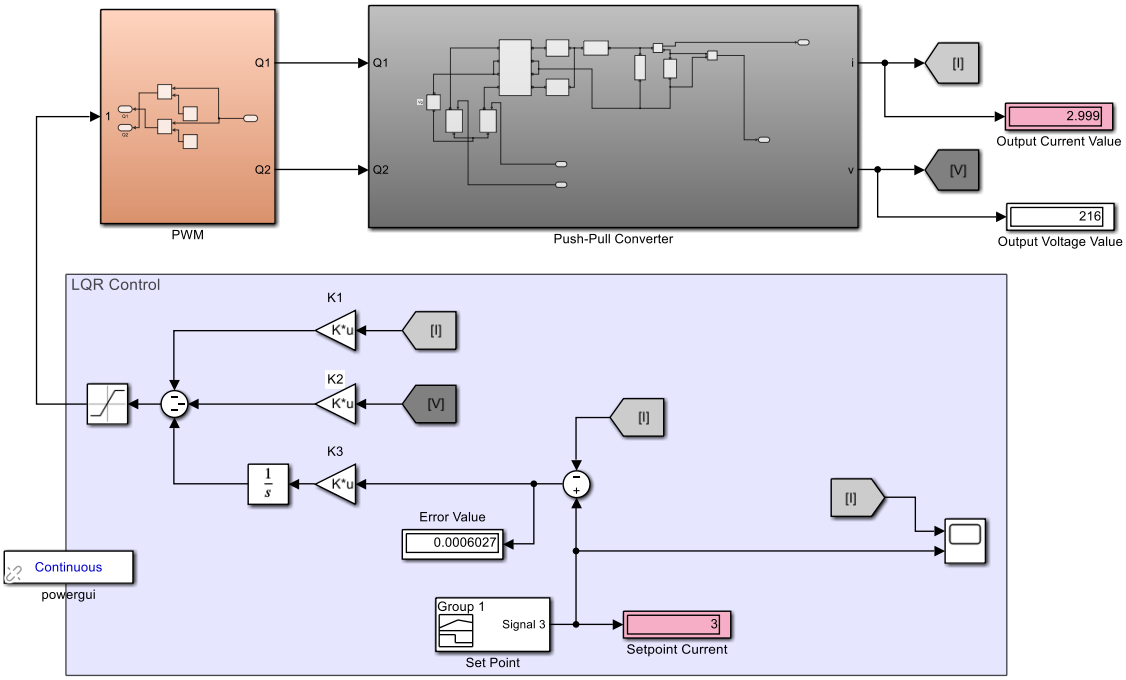


Figure 3.12: Push-Pull DC-DC converter controlled with LQR controller

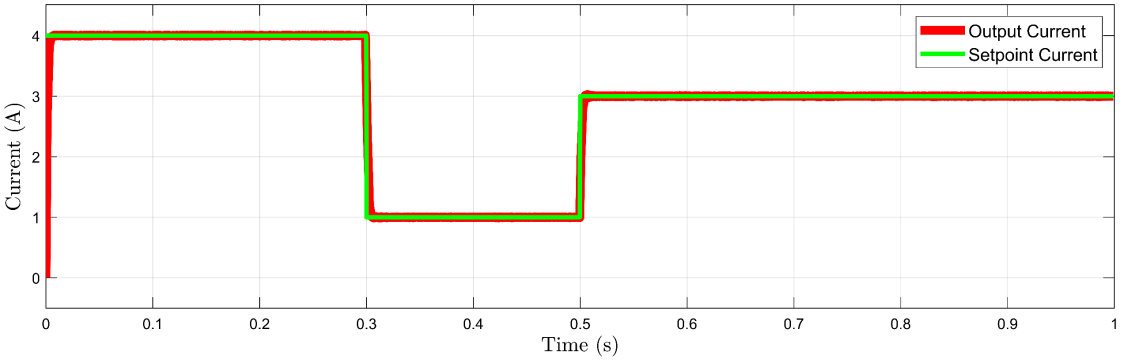


Figure 3.13: Push-Pull DC-DC converter curves in close loop (LQR controller)

From Figure 3.13 , it's evident how the LQR controller effectively minimizes the response time when faced with sudden set point variations , ensuring swift and accurate adjustments to maintain desired current levels.

### LQR Controller based Current Observer

A push-pull converter controlled with Linear Quadratic Regulator with Integrator action (LQI) controller plus observer present an Figure 3.14.

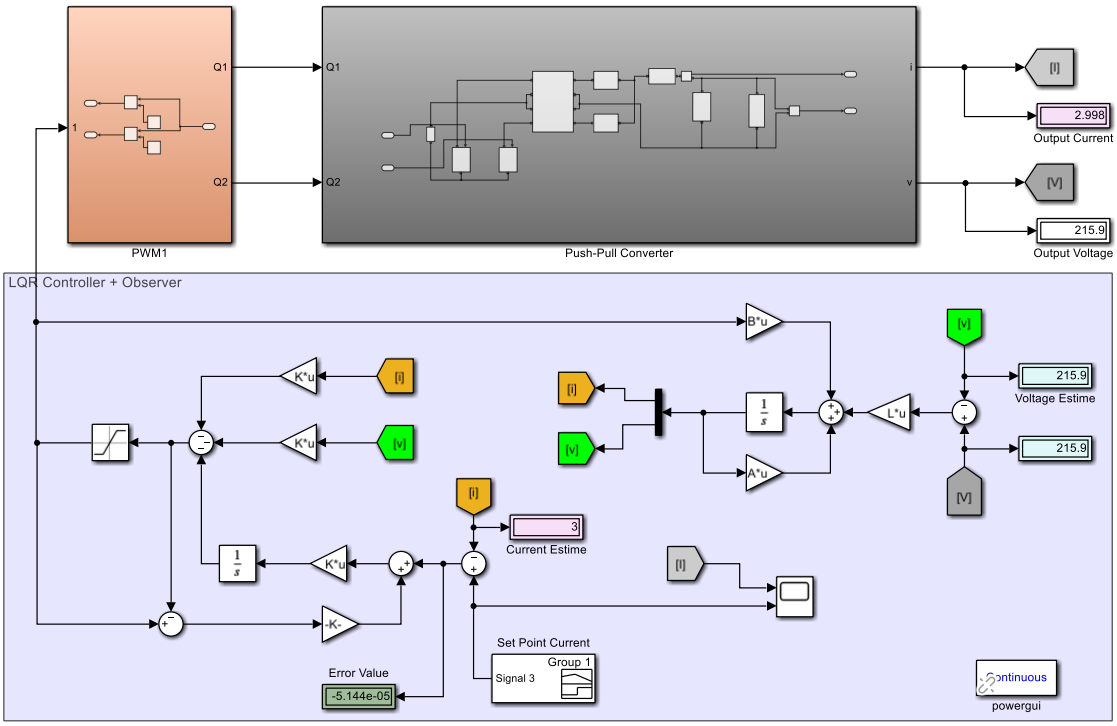


Figure 3.14: Push-Pull DC-DC converter controlled with LQR controller plus observer

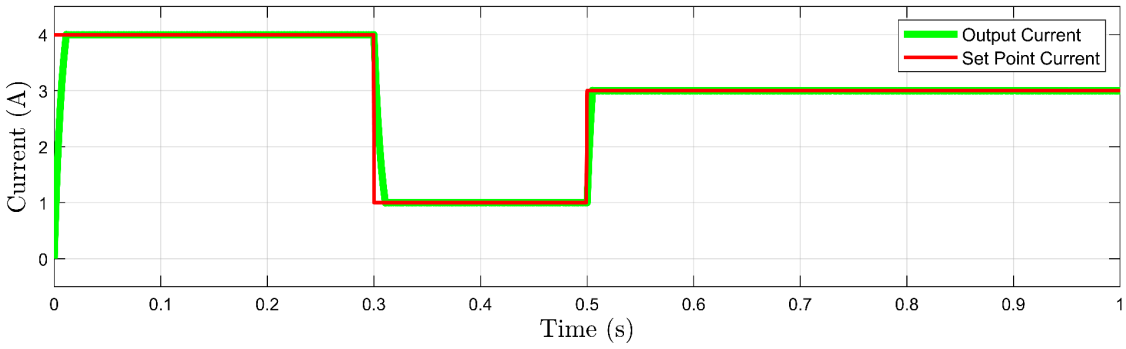


Figure 3.15: Push-Pull DC-DC converter curves in close loop (LQR controller plus observer)

Figure 3.15 presents current curves of the estimated current of push-pull converter and its reference, from this figure, one can see the tracking of the estimated current with its set point.

## 3.5 Simulation of the PV Emulator

This section details simulations of the ANN-based photovoltaic emulator (PVE) incorporating with two different methods PID ( Figures 3.16), LQR (Figures 3.17) controller and LQR based current observer (Figures 3.18) . To assess the robustness of the proposed PV ANN emulator, to test this many variations are made of irradiance, temperature and load.

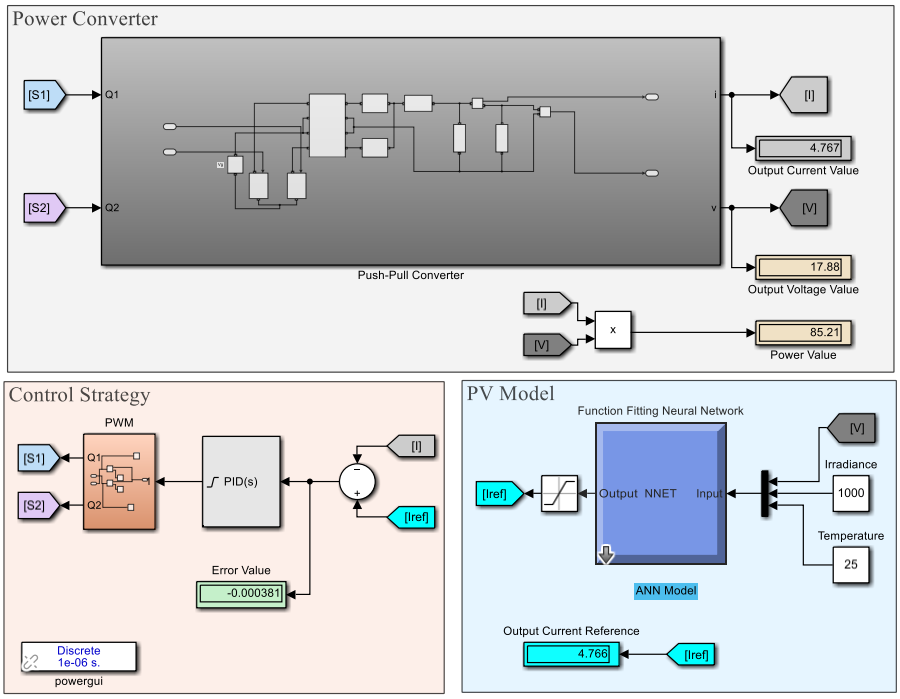


Figure 3.16: The ANN-based PV emulator controlled with PID

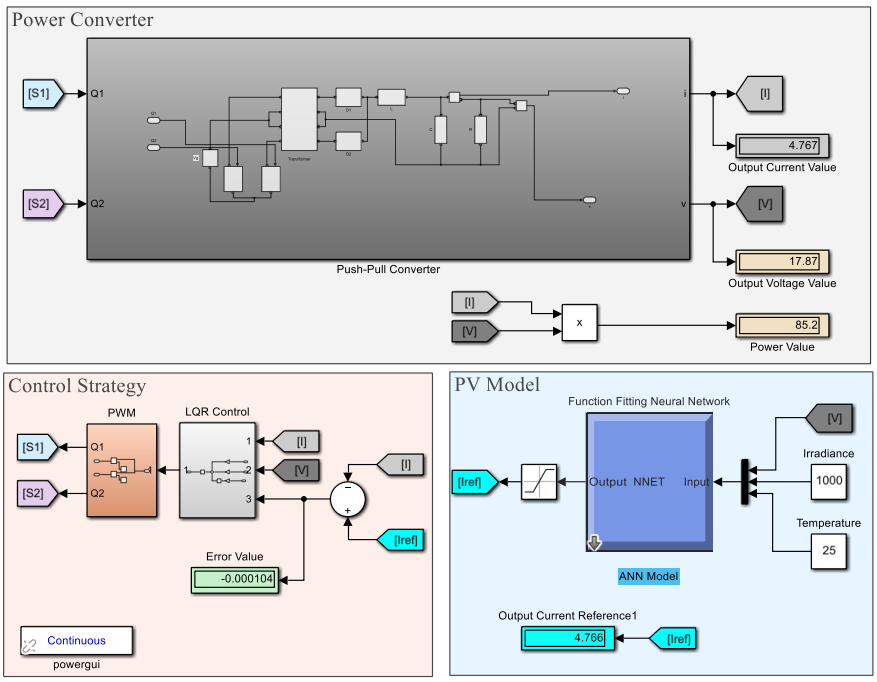


Figure 3.17: The ANN-based PV emulator controlled with LQR

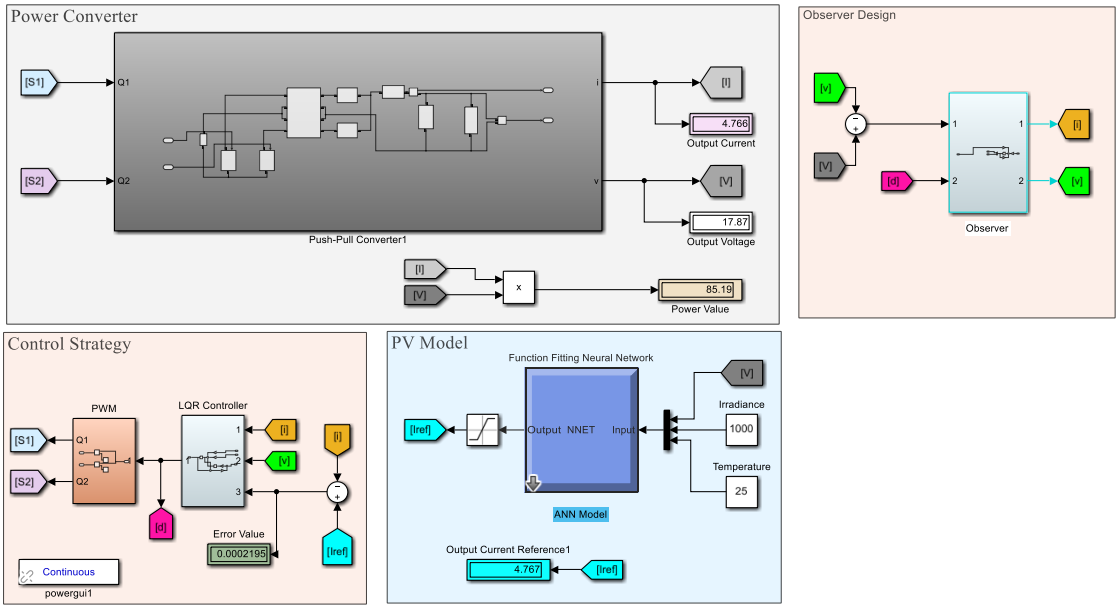


Figure 3.18: The ANN-based PV emulator controlled with LQR based Observer

### 3.5.1 PV Emulator Under Sudden Changes of Irradiance

To show the effectiveness of our proposed PV ANN model a comparison between PV electrical model and our proposed model (PID and LQR) in the same conduction of load and temperature under sudden change of irradiance Figure 3.19.(a).

For this context the load is set to 3.75 Ω and irradiance: from 400 W/m² to 1000 W/m² at t=0.15s, and from 1000 W/m² to 800 W/m² at t=0.35s.

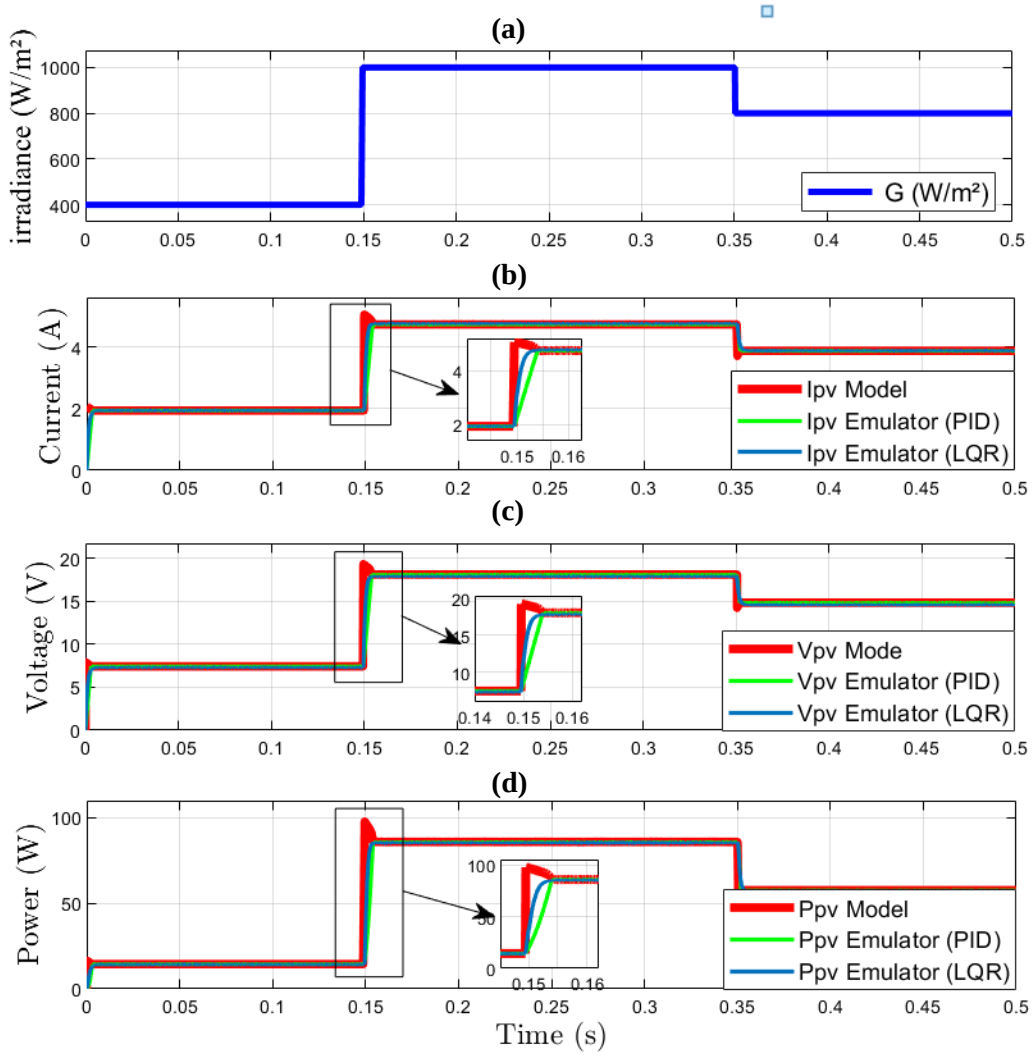


Figure 3.19: PV emulator under Irradiance effect

Under sudden changes of irradiance and from Figure 3.19 we conclude that the PV ANN emulator characteristics align closely with the electrical PV model. This serves as confirmation that the proposed ANN-based PVE operates effectively with LQR Controller.That confirmed the performance of LQR compared to PID controller.

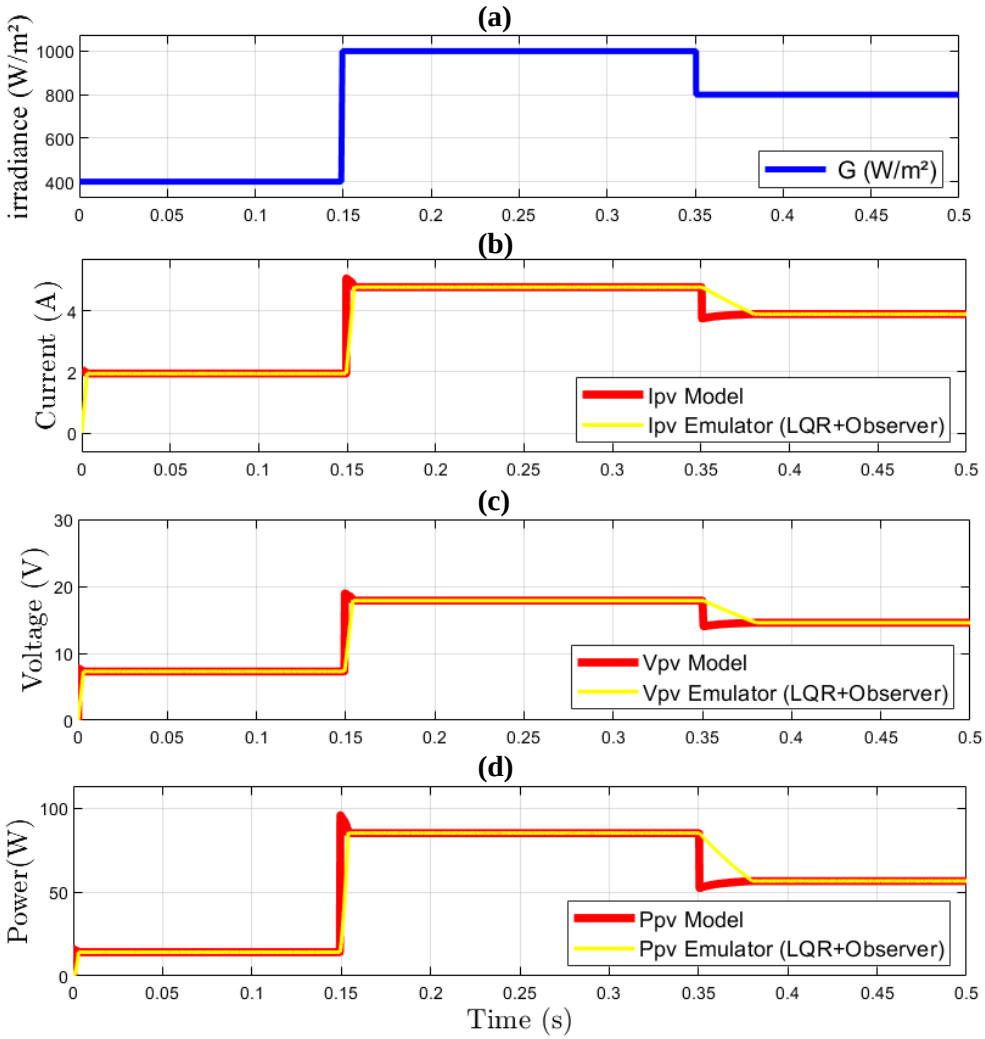


Figure 3.20: PV emulator (LQR plus Observer) under Irradiance effect

Figure 3.20 presents the comparison curves between PV electrical model and PVE when the latter controlled by LQR strategy with the add of current observer, the whole system under sudden Changes of Irradiance. From this figure we can see the matching form curves between the current reference and the estimated current, and the system (PVE) until work correctly.

### 3.5.2 PV emulator under sudden changes of Temperature

In this subsection the temperature was varied in two steps: from $15^oC$ to $30^oC$ at 0.15s and from $30^oC$ to $45^oC$ at 0.35s.

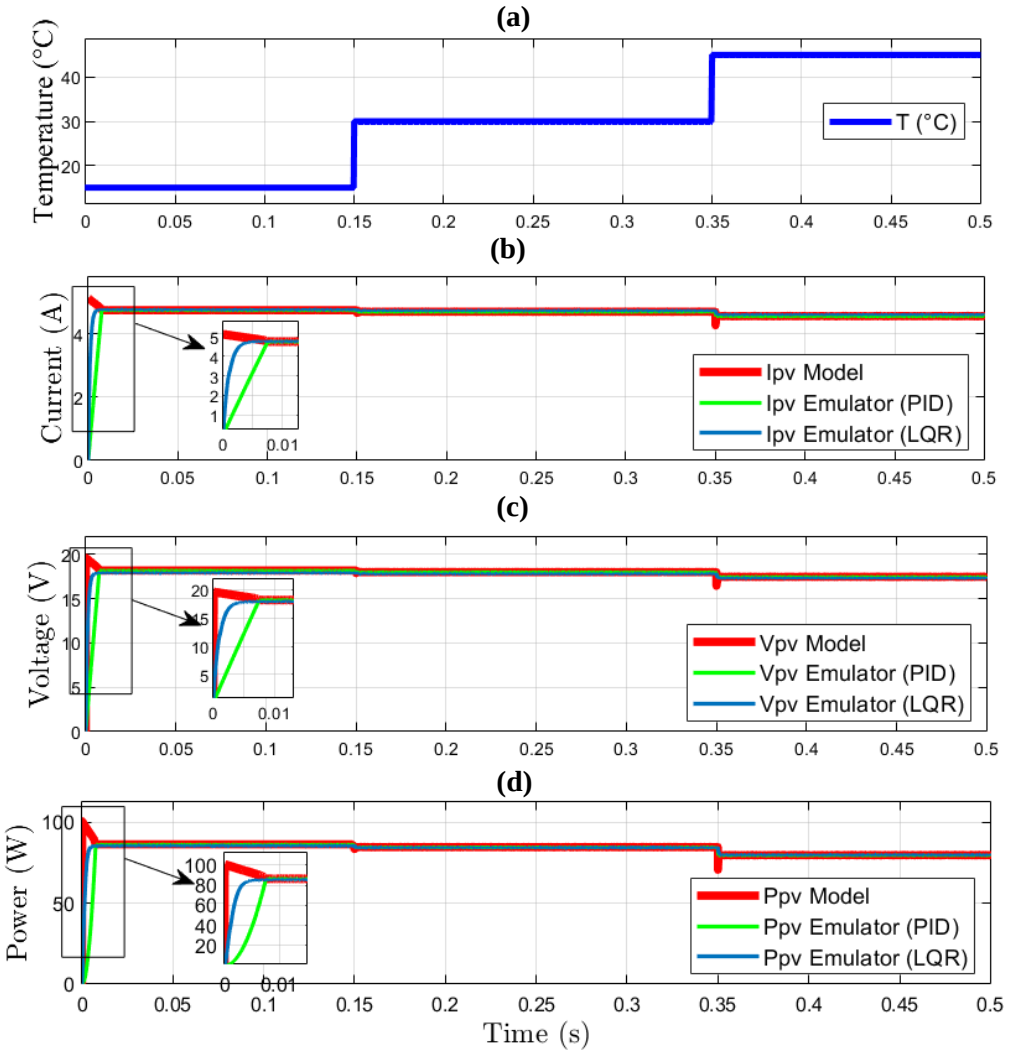


Figure 3.21: PV emulator under Temperature effect

Under sudden changes of temperature and from Figure 3.21 show that the emulator behavior closely matches the predictions of the electrical model. This confirms the effectiveness of the proposed ANN-based PVE design with LQR Controller.That confirmed the performance of LQR compared to PID controller.

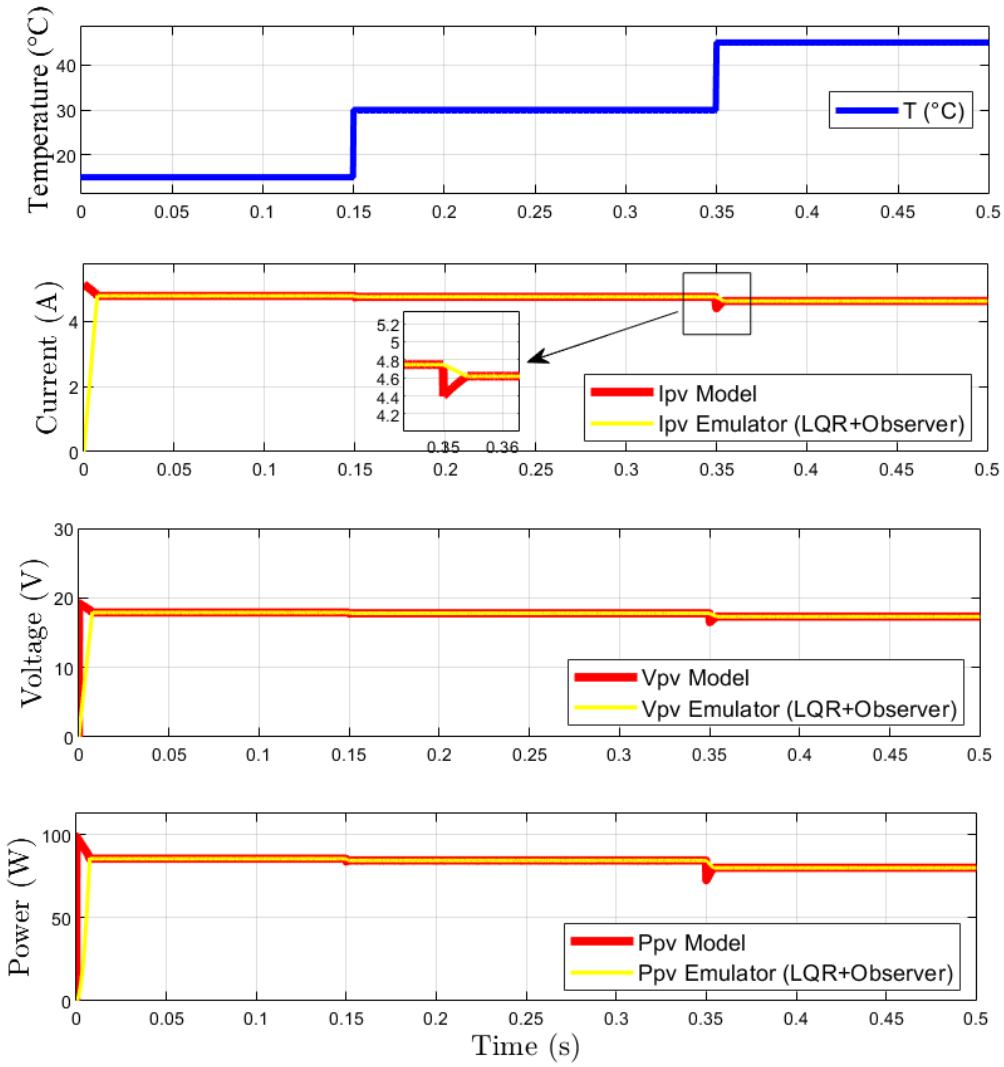


Figure 3.22: PV emulator (LQR plus Observer) under Temperature effect

Figure 3.22 presents the comparison curves between PV electrical model and PVE when the latter controlled by LQR strategy with the add of current observer, the whole system under sudden Changes of temperature. From this figure we can see the matching form curves between the current reference and the estimated current, and the system (PVE) until work correctly.

### 3.5.3 PV emulator under Load variation

The next subsection compares the proposed PV emulator to the electrical PV model panel under varying load conditions in such way to cover all load points.

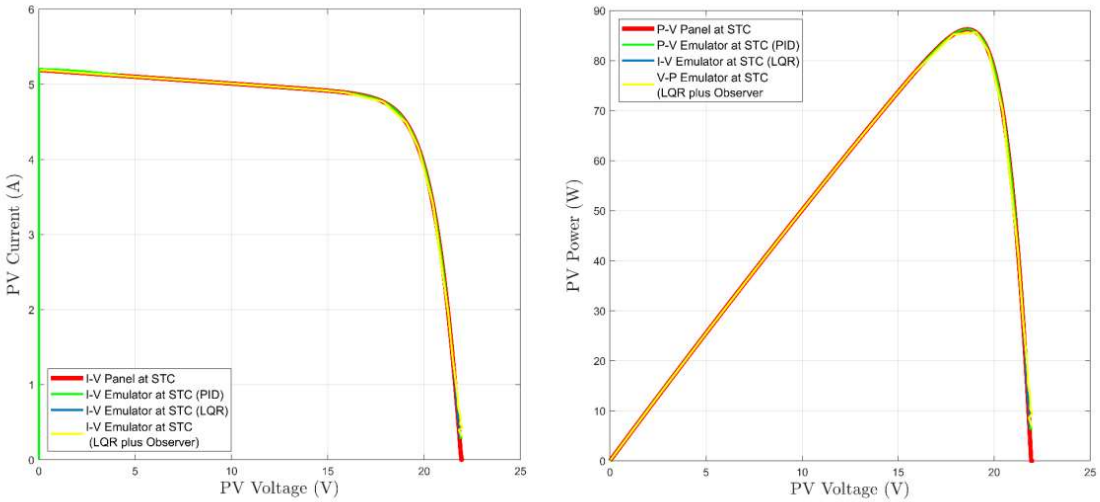


Figure 3.23: I-V and P-V curves of PV and PVE.

As shown in Figures 3.23, the performance results indicate that the emulator's characteristics closely match those of the PV panel's electrical model at Standard Test Conditions (STC), confirming the proposed emulator's effectiveness.

## 3.6 Conclusion

In this chapter, a ANN PV emulator utilizing a DC-DC push-pull converter is controlled, through two different methods PID, LQR and LQR associated with current observer. Various performance tests were conducted on the proposed emulator to evaluate its dynamic behavior, speed, and overall viability. The simulation results and the proposed ANN-based PVE demonstrate that it is a fast and accurate PV emulator with straight forward real-time control. Additionally, it exhibits a quick dynamic response and highly stable output. The system is also capable of emulating any operating point on the PV curve.

# General Conclusion

In this study, we concentrated on the development, modeling, and simulation of artificial neural network photovoltaic emulator utilizing a push-pull converter.

The first chapter provided comprehensive definitions and background information on photovoltaic emulators and DC-DC converters, establishing a solid foundation for our research. In the second chapter, we explored the modeling and control aspects of the push-pull converter by LQR strategy associated with current observer to ensure a thorough understanding of its behavior and operation.

In the third chapter, extensive simulations and validations demonstrate the effectiveness and accuracy of our PV emulator. The results were highly satisfactory, confirming the successful implementation of our proposed system. The ANN-based PV emulator exhibited excellent performance in replicating the behavior of a real photovoltaic system, enabling reliable and efficient testing of various power electronics applications and control strategies.

Overall, this research contributes significantly to the field of photovoltaic emulation and provides valuable insights into the modeling and control of push-pull converters. The developed ANN-based PV emulator controlled by LQR controller in the association with current PVE emulator presents a robust and accurate tool for experimental investigations, allowing researchers and engineers to explore and optimize the performance of power electronics systems connected to photovoltaic sources. Future research can focus on expanding the scope of applications and exploring additional control strategies to enhance the versatility and functionality of the PV emulator.

Finally, we wish the next generation to move on to the experimental validation of the proposed ANN PV Emulator. It is imperative that future researchers take the theoretical advancements and simulated results into real-world scenarios to evaluate

performance under practical conditions. This step will not only verify the robustness of the proposed system but also provide insights into potential areas for improvement and innovation. The transition from simulation to physical implementation will help in identifying unforeseen challenges and refining the design for better efficiency and reliability.

# Appendix

## Mathematical Modeling

This project references a real solar panel: the Solar-world SW 85 poly R5A/D . The electrical specifications of these panel is detailed in the following table.

| | |
|---|---|
| maximum power ($P_{max}$) | 85 W |
| Voltage at maximum power ($V_{MP}$) | 17.9 V |
| current at maximum power ($I_{MP}$) | 4.77 A |
| Open circuit voltage ($V_{oc}$) | 22 V |
| Short circuit current ($I_{sc}$) | 5.20 A |

Specification of Solar World panel parameters.


(a) (b)

Figure 3.24: (a). PV Panel parameter, (b). Solar world SW 85 poly R5A/D

# Bibliography


[1] Razman Ayop and Chee Wei Tan. A comprehensive review on photovoltaic emulator. Renewable and Sustainable Energy Reviews, 80:430–452, 2017.

[2] Khiem Nguyen-Duy, Arnold Knott, and Michael A. E. Andersen. High dynamic performance nonlinear source emulator. IEEE Transactions on Power Electronics, 31(3):2562–2574, 2016.

[3] Saraswathi Kalaimohan Thankanadar Arumugam Parassuram V. Swaminathan Gurunandh Periasamy Somasundaram Sudhakar, Kumarasamy. An artificial neural network-based comprehensive solar photovoltaic emulator. International Journal of Photoenergy, 2022:14, 2022.

[4] BENMEHIRIS Makhlouf TOUHAMI Oussama. Study and simulation of pv emulator based on dc-dc push-pull converter. Master's thesis, University of Amar Telidji- Laghouat, Juin 2023.

[5] F. Gómez-Castañeda, G. M. Tornez-Xavier, L. M. Flores-Nava, O. Arellano-Cárdenas, and J. A. Moreno-Cadenas. Photovoltaic panel emulator in fpga technology using anfis approach. In 2014 11th International Conference on Electrical Engineering, Computing Science and Automatic Control (CCE), pages 1–6, 2014.

[6] M.C. Di Piazza, M. Pucci, A. Ragusa, and G. Vitale. Analytical versus neural real-time simulation of a photovoltaic generator based on a dc-dc converter. In 2009 IEEE Energy Conversion Congress and Exposition, pages 3350–3356, 2009.

[7] Younghyun Lee and Jonghwan Lee. Solar power prediction modeling based on artificial neural networks under partial shading. Applied Sciences, 13(18), 2023.

[8] Engin Karatepe, Mutlu Boztepe, and Metin Colak. Neural network based solar cell model. Energy Conversion and Management, 47(9):1159–1178, 2006.

[9] Chen Zhang Ming Yang Siyi Wang, Yunpeng Zhang. Improved artificial neural network method for predicting photovoltaic output performance. Global Energy Interconnection, 3:553–561, 2020.

[10] Shoba Ranganathan Michael Gribskov Kenta Nakai Christian Schönbach. Encyclopedia of bioinformatics and computational biology. pages 612–620, 2019.

[11] Sushamshushekar Doddabasappa. Lqr control design for a dc-dc converter using sensitivity functions. Master Thesis, 2019.

[12] Lung-Sheng Yang, Tsorng-Juu Liang, and Jiann-Fuh Chen. Transformerless dc–dc converters with high step-up voltage gain. IEEE Transactions on Industrial Electronics, 56(8):3144–3152, 2009.

[13] L. Umanand. POWER ELECTRONICS: ESSENTIALS & APPLICATIONS (With CD ). Wiley India Pvt. Limited, 2009.

[14] Hadi Tarzamni, Homayon Soltani Gohari, Mehran Sabahi, and Jorma Kyyrä. Nonisolated high step-up dc–dc converters: Comparative review and metrics applicability. IEEE Transactions on Power Electronics, 39(1):582–625, 2024.

[15] Yavuz Koç, Yaşar Birbir, and Hacı Bodur. Non-isolated high step-up dc/dc converters – an overview. Alexandria Engineering Journal, 61(2):1091–1132, 2022.

[16] Raksha Adappa and Suryanarayana K. Modeling and analysis of 1.2 kw, 36–375 v, push–pull converter. Advances in Renewable Energy and Electric Vehicles, 767, 2022.

[17] V.T. Ranganathan M. B. Patil, V. Ramanarayanan. Simulation of Power Electronic Circuits. Reprint, Reprint 2013.

[18] Nurul Fitri Muthmainnah, Adnan Rafi Al Tahtawi, and Baisrum Baisrum. Voltage stability control of boost converter using linear quadratic integrator. Journal of Fuzzy Systems and Control, 1(2):39–43, Aug. 2023.

[19] Ali Niknezhadi, Miguel Allué-Fantova, Cristian Kunusch, and Carlos Ocampo-Martínez. Design and implementation of lqr/lqg strategies for oxygen stoichiometry control in pem fuel cells based systems. Journal of Power Sources, 196(9):4277–4282, 2011. CONAPPICE 2010.

[20] Ammar Falah Preview author details Abbas, Nizar Hadi; Algamluoli. Designing an integral lqr controller for dc-dc x-converter based on enhanced shuffled frog-leaping optimization algorithm. Journal of Electrical Systems Preview publication details, 16(2):152–170, 2020.

[21] Anbarasi MP; Kanthalakshmi S. Linear quadratic optimal control of solar photovoltaic system: An experimental validation. Journal of Renewable and Sustainable Energy, 8, 2016.

[22] K. Ogata. Modern Control Engineering. Instrumentation and controls series. Prentice Hall, 2010.

[23] Nabil A. Ahmed. Modeling and simulation of ac–dc buck-boost converter fed dc motor with uniform pwm technique. Electric Power Systems Research, 73(3):363–372, 2005.

[24] ÜMİT ÖNEN ABDULLAH ÇAKAN İLHAN İLHAN. Performance comparison of optimization algorithms in lqr controller design for a nonlinear system. Turkish Journal of Electrical Engineering and Computer Sciences, 16:1938–1953, 2019.